# THE INFLUENCE OF LOW LEVELS OF ALUMINA ON THE ATTRITION RESISTANCE AND FISCHER-TROPSCH SYNTHESIS PERFORMANCE OF A PRECIPITATED IRON CATALYST

Thesis submitted for the Taught Masters in Catalysis degree in the Department of Chemical Engineering at the University of Cape Town

by

Hermanus Antonie Lombard

Hons. B.Sc. (Chemistry) UNISA



Promotor: Prof. E van Steen

Cape Town

2004

**Abstract**

The addition of alumina as a binder to a spray-dried, iron-based Fischer-Tropsch catalyst was investigated. Alumina was either added during the precipitation or just prior to spray-drying in the form of aluminium nitrate. The addition of up 1.0 $Al_2O_3$/100Fe, as aluminium nitrate, to the precipitated iron catalysts caused a decrease in the impact attrition resistance of the catalysts upon spray-drying and calcination at 350°C. The catalyst with the aluminium added during the precipitation step had the lowest attrition resistance. Relatively small decreases in the mean particle size (the largest difference being from 49 μm to 40μm), of the catalysts indicate that the mechanism of attrition observed was abrasion rather than break-up. The BET surface area increased slightly with an increase in the aluminium content of the catalysts.

No significant differences in the overall activity, measured by the CO conversion (ca. 87%), or the FT activity (ca. 44%), as measured by the $CO+CO_2$ conversion, of the catalysts were observed. The catalyst with the aluminium added during the precipitation step seemed to possess an increased hydrogenation ability as measured by the increase in the selectivity towards $CH_4$ and $C_2H_6$. This catalyst also displayed an earlier onset of reduction in a TPR analysis. The rate of the water gas shift reaction decreased in both the catalysts that contained aluminium.

**TABLE OF CONTENTS**

**1 LITERATURE REVIEW**

# 1 LITERATURE REVIEW

## 1.1 INTRODUCTION

In the Fischer-Tropsch process carbon monoxide (CO) and hydrogen ($H_2$) is converted into a mixture of hydrocarbons. The CO and $H_2$ gas mixture is commonly referred to as synthesis gas (Storch et al., 1951; Dry, 1996). Synthesis gas can be obtained from natural gas, after reforming of the methane, or from the gasification of coal or biomass. The Fischer-Tropsch process has thus become a major route for converting natural gas, heavy oil residues, coal or biomass into liquid hydrocarbons. Schematically the possible process routes for obtaining synthesis gas and the conversion of synthesis gas into valuable products is shown in Figure 1.1.

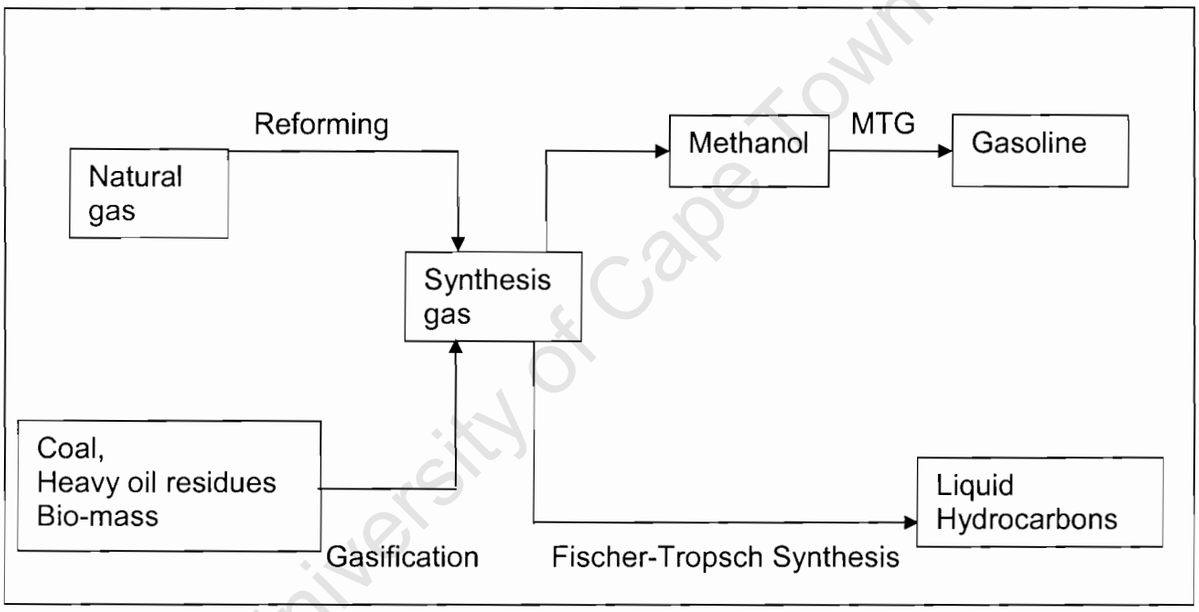




**Figure 1.1:** Possible pathways to convert natural gas, heavy oil residue, coal and biomass via the generation of synthesis gas into valuable chemicals and liquid hydrocarbons (adapted from van der Laan, 1999).

Natural gas, coal and crude oil are classified as fossil fuels. They can be converted into synthesis gas by reforming or gasification. The reserves of coal are approximately six times higher than that of oil and natural gas combined (Dry, 1996). Hence coal will continue to play a major role to play in future syngas production.

The conversion of natural gas into liquid hydrocarbons allows for the utilisation of remote natural gas sources by converting them into fuels and chemicals (Rostrup-Nielsen, 2002; van der Laan, 1999.)

Amongst the fossil fuels, natural gas is the cleanest burning fuel. Coal has complicated chemical structures, and during the combustion, pyrolysis or gasification of it, potentially harmful products are released into the environment.

In the steam reforming process methane is converted into CO and $H_2$ over catalysts containing nickel on alumina or the aluminates of calcium or magnesium. The process is endothermic and occurs at temperatures up to 1173 K in the presence of steam (Kochloefl,1997).

In the gasification process CO and $H_2$ is produced by the combustion of coal or biomass with only enough oxygen to convert the carbon to CO and $H_2$, not to $CO_2$.

Synthesis gas can be converted into methanol over a $Cu/ZnO/Al_2O_3$ catalyst (Chinchen et al., 1990). Methanol can subsequently be converted to gasoline over an acid catalyst, such as the zeolite HZSM 5.

The Fischer-Tropsch reaction represents another process to convert synthesis gas into liquid products. The Fischer-Tropsch synthesis has been recognised as a heterogeneous surface catalysed polymerisation reaction (Friedel and

Anderson, 1950). During this reaction carbon monoxide is hydrogenated over certain transition metals to form $CH_3$, $CH_2$ and CH species on the surface of the metal. The insertion of the $CH_2$ species into other surface species leads to chain growth and the subsequent formation of various hydrocarbon products by desorption from the catalyst surface.

During the industrial application of the Fischer-Tropsch process the catalyst particle, mainly iron or cobalt based, is subjected to attrition. The mechanism, influence and minimisation of attrition, and the influence of a binder on synthesis behaviour, for iron based catalysts are the focus areas of this thesis. A model precipitated iron catalyst system was chosen for this study due to the ease of preparing the various catalyst samples needed.

### 1.1.1 A SHORT HISTORY OF THE FISCHER-TROPSCH PROCESS

The following discussion on the history and development of the Fischer-Tropsch process is based on articles by Dry (1981, 1996 and 2002) unless stated otherwise.

As far back as 1902 it was observed that methane was formed from mixtures of $H_2$ and CO over nickel and cobalt catalysts. The company BASF then produced liquid products over a cobalt catalyst by using high pressures (BASF German Patent 293 787, 1913).

In 1923 Fischer and Tropsch used alkalised iron as a catalyst at pressures of 100 to 150 bar and obtained liquid products rich in oxygenates. They observed that by decreasing the reaction pressure hydrocarbons were formed, however the iron catalyst deactivated rapidly. Most of the subsequent research focused on developing nickel and cobalt catalysts for use at lower pressures. The use of nickel was eventually discontinued because of its high selectivity towards methane and losses as nickel carbonyl from reactors.

In 1936 four Fischer-Tropsch plants were commissioned in Germany, with a total hydrocarbon capacity of about 200 ktons per year. By 1944 their potential capacity was about 700 ktons per year from nine reactors. The catalyst used in these plants was based on cobalt.

Research on the application of iron-based catalysts continued unabated and in 1936 Pichler found that the lifetime of iron based catalyst was markedly improved by increasing the operating pressure from atmospheric pressure to about 15 bar. This ensured further development work on iron as a catalyst for the Fischer-Tropsch process.

In 1943 comparative tests between iron and cobalt based catalysts were performed at Schwarzheide and despite apparently successful results for the iron-based catalysts, the industrial catalyst of choice remained cobalt. The Fischer-Tropsch synthesis with a cobalt-based catalyst supplied Germany with gasoline during the Second World War. The plants were decommissioned at the end of World War 2.

In 1944 Japan also operated three Fischer-Tropsch plants with a capacity of 100 ktons per year.

During the 1940's the perception was that the reserves of crude oil were being depleted and that an increase in the price of crude oil would follow. Therefore, the development of Fischer-Tropsch technology continued after the Second World War. Two German firms, Rührchemie and Lurgi, formed an *Arbeitsgemeinschaft* (ARGE) and they developed a fixed bed reactor using a precipitated iron catalyst for the production of waxes. In the USA fluidised bed reactor technology for the Fischer –Tropsch synthesis was developed. Kellogg Co. investigated a circulating entrained catalyst reactor. The fluidised bed reactors produced high yields of gasoline.

In South Africa a decision was made to invest in the Fischer-Tropsch process as a means of obtaining oil from coal and the company SASOL was formed. In 1955 the Sasol One plant was commissioned with both the ARGE and the entrained bed Kellogg reactors.

The discovery of large oil deposits in the Middle East during the mid 1950's led to a decrease in the price of crude oil and interest in the Fischer-Tropsch process waned. However Sasol One continued its operations. After numerous modifications, both mechanically and operational, and considerable catalyst development, the Kellogg reactors at the Sasol One plant were operated commercially.

The oil crisis in 1973 rekindled interest in the Fischer-Tropsch process. Two further plants, Sasol Two and Sasol Three, were erected to supply gasoline, from coal based derived synthesis gas, to South Africa. They used the Kellogg's modified Circulating Fluidised Bed (CFB), technology and the production capacity was 4200 ktons per year, yielding mainly ethylene, gasoline and diesel.

In 1985 Mobil erected a Methanol to Gasoline, MTG, plant in New Zealand, using natural gas as feedstock. The methane in the natural gas was converted to syngas and then to methanol. The methanol was then converted into gasoline over a zeolite catalyst. The plant had a capacity of approximately 600 ktons per year.

Mossgas in South Africa and the Shell plant at Bintuli in Malaysia came on line during 1992 and 1993 with off-shore natural gas as feed. Methane is converted into synthesis gas using either steam-reforming or partial oxidation. Mossgas uses the Circulating Fluidised Bed technology with a fused iron catalyst. The capacity is ca. 900 ktons per year. Shell utilises fixed bed reactor technology with a cobalt-based catalyst. The capacity of the plant at Bintuli is ca. 600 ktons per year.

At the Sasol Two and Three plants the Circulating fluidised bed reactors were replaced at the end of the 90's with fixed fluidised beds with a projected total capacity of 124 000 bbl/day (Steynberg et al., 1999).

### 1.1.2 REACTIONS IN THE FISCHER-TROPSCH SYNTHESIS

The basic Fischer-Tropsch reaction is the hydrogenation of CO with $H_2$ over certain transition metals (Dry, 1996).

$$CO + H_2 \rightarrow CH_2 + H_2O \quad \text{.....(1.1)}$$

The $CH_2$ units then form a wide range of hydrocarbons, mainly olefins by a surface polymerisation reaction. The heat of the reaction is ca. 146 kJ per mole reacted carbon atom.

Frohning et al. (1980) and Jager (1998) presented the Fischer-Tropsch reactions leading to the formation of alkanes (1.2) and alkenes (1.3) as follows:

$$nCO + (2n+1)H_2 \leftrightarrow C_nH_{2n+2} + nH_2O \quad \text{.....(1.2)}$$

$$nCO + 2nH_2 \leftrightarrow C_nH_{2n} + nH_2O \quad \text{.....(1.3)}$$

$\Delta H_{rxn,500K}$ = -167 kJ/mole

From reactions 1.1, 1.2 and 1.3, it can be seen that for each mole of CO reacted one mole of water is also formed. Water is thus a major by-product of the Fischer-Tropsch process.

From reactions 1.1,1.2 and 1.3 it can be seen that the Fischer Tropsch reaction is highly exothermic and effective heat removal is important for reactor temperature control. Slurry bubble column reactors and fixed fluidised bed reactors, with their high degree of mixing are very effective in removing the heat of the reaction (Dry, 1996).

The formation of the commonly found oxygenated compounds may be presented by the following reactions (Dry, 1981):

Alcohols: $2nH_2 + nCO \leftrightarrow C_nH_{2n+2}O + (n-1)H_2O$.....(1.4)

Aldehydes and Ketones: $2(n-1)H_2 + nCO \leftrightarrow C_nH_{2n}O_2 + (n-1)H_2O$.....(1.5)

Acids: $(2n-1)H_2 + nCO \leftrightarrow C_nH_{2n}O_2 + (n-1)H_2O$ .....(1.6)

An overall picture of the thermodynamics of the reactions mentioned is given in Figure 1.2. The formation of methane is highly favoured, whereas the formation of alkynes is not favoured due to the positive free energy change. Fortunately the thermodynamic equilibrium is reached slowly and by the selection of appropriate promoters and process condition the formation of certain hydrocarbons can be favoured (Dry, 1981).

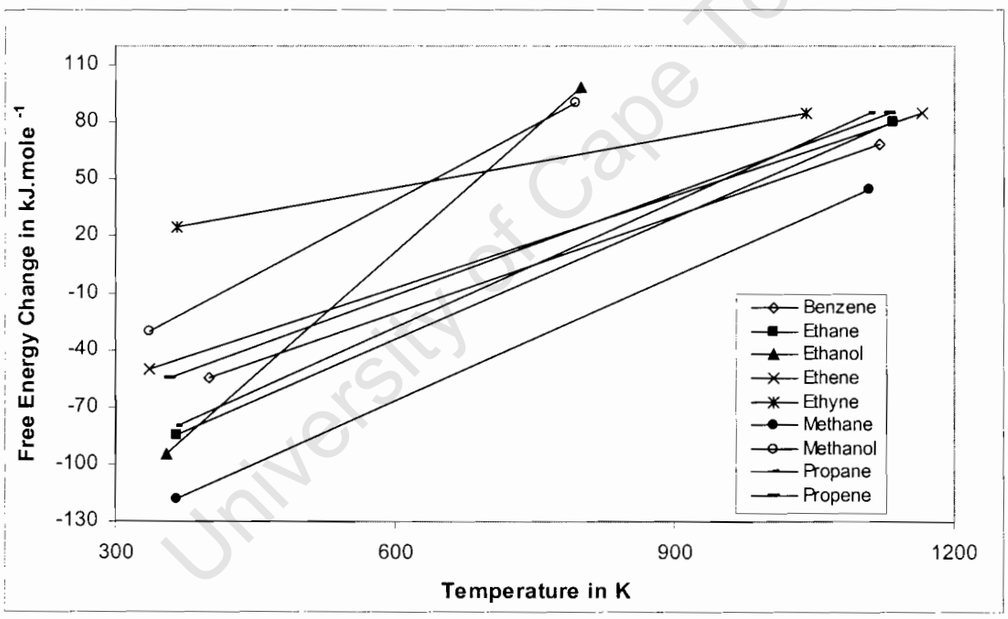




**Figure 1.2:** Standard free energies of formation for the synthesis of hydrocarbons and alcohols (Redrawn from Denny and Whan, 1978).

In the Fischer-Tropsch synthesis catalysed by iron-based catalysts, the water gas shift reaction also occurs (Frohning 1980; van der Laan, 1999). In the water gas shift reaction CO is converted to $CO_2$. This is an undesirable by-product.

$CO + H_2O \leftrightarrow CO_2 + H_2$ ……..(1.7)

$\Delta H^{rxn}(603\ K) = -38.6$ kJ/mole

The water-gas shift reaction is typically at thermodynamic equilibrium in iron-catalysed Fischer-Tropsch synthesis performed at temperatures above 523 K (Satterfield and Huff, 1982; Zimmerman and Bukur, 1990).

## 1.2 PROCESSES FOR THE FISCHER-TROPSCH SYNTHESIS

The iron catalysed Fischer-Tropsch synthesis is conducted commercially at elevated temperature and pressures. The two main operation modes currently used are based on the temperature regime in which the process is applied, i.e. high temperature and low temperature synthesis (Dry, 2002). The pressure range applied in both operation modes varies between 25 and 50 bar (Dry, 1996).

### 1.2.1 High Temperature Fischer-Tropsch Process

In the high temperature Fischer-Tropsch (HTFT) mode the typical temperature range is between 300°C and 350°C. Fused iron catalysts are used. Cobalt catalysts are not used at these temperatures due to the high selectivity towards methane formation. In this temperature range low molecular mass gaseous products, olefins, paraffins and gasoline are obtained. Fixed fluidised bed and circulating fluidised bed reactors are used.

#### 1.2.1.1 Fluidised Bed Processes

In the fixed fluidised bed reactor the catalyst remains in the reaction zone of the reactor and the synthesis gas passes upwards through it, keeping the catalyst bed fluidised. The gas velocity must be more than the minimum fluidisation velocity in order to fluidise the catalyst bed. If the gas velocity is too high the catalyst will be elutriated. Reaction heat is removed by cooling coils and the product gas. Fine catalyst particles, which are elutriated, are separated from the product gas by cyclones. The Fischer-Tropsch catalyst used in this process is a fused iron catalyst.

#### 1.2.1.2 Circulating Fluidised Bed Process

In the circulating fluidised bed reactor, such as used by Mossgas (Steynberg et al., 1999) and used by Sasol up to the late 90's, the catalyst is entrained in a fast moving synthesis gas stream into the reaction zone, carried out of the reactor, separated from the gas phase and re-circulated. The finer catalyst particles are separated from the product gas via cyclones and added to the catalyst inventory. Reaction heat is removed by cooling coils and the product gas. The catalyst used in this process is a fused iron catalyst. (Dry, 1981; Dry, 2002).

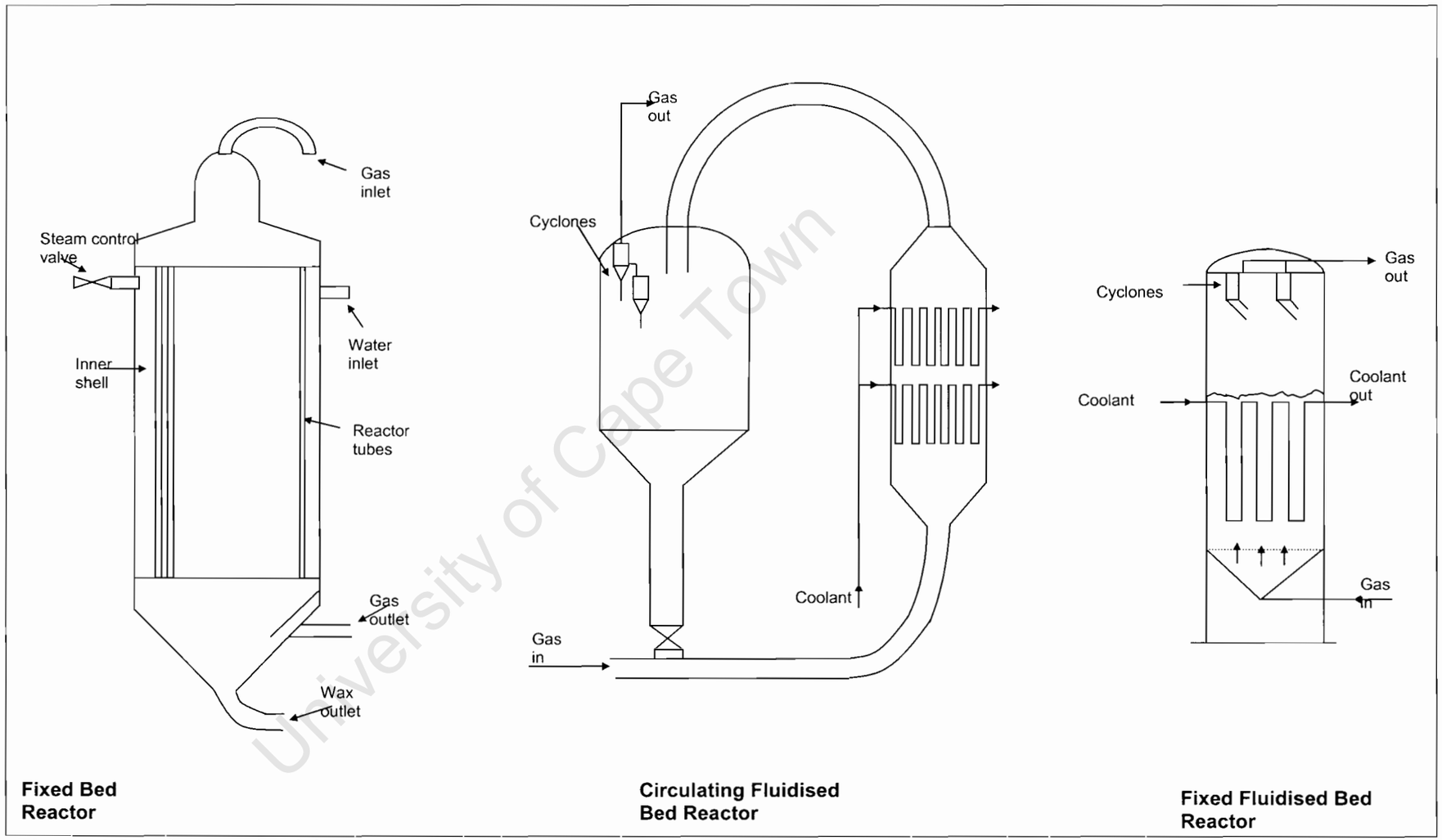




**Figure 1.3:** Schematic of the reactor types in commercial use.

### 1.2.2 Low Temperature Fischer-Tropsch Process

In the low temperature Fischer-Tropsch (LTFT) mode the typical temperature range is between 200°C and 240°C. Precipitated iron and supported cobalt catalysts are used. In this temperature range high molecular mass linear waxes are produced. Fixed bed and slurry bed reactors are typically used.

In the fixed bed reactor the catalyst is packed in long narrow tubes contained in a reactor. Cooling water is then passed around the tubes and steam generated by heat exchange. Controlling the pressure of the steam controls the temperature in the reactor. High recycle ratios are also used to help control the reaction temperature. An advantage of these reactors is that in the case of a catalyst poison such as $H_2S$ entering the reactor, only the first section of the catalyst bed is affected.

In the slurry bed reactor the catalyst is suspended in a liquid which has a low vapour pressure at the temperature being used. The synthesis gas is passed through it. The reaction heat is removed by cooling coils (Dry, 1981; Dry, 2002).

## 1.3 PRODUCTS FORMED IN THE FISCHER-TROPSCH SYNTHESIS

### 1.3.1 Origin of Products

In the Fischer-Tropsch reaction various products are produced. These vary from methane, longer chain n-paraffins, 1-olefins, branched hydrocarbons, up to high boiling waxes. Oxygenated chemicals such as alcohols, ketones, aldehydes, carboxylic acids and water are also formed.

Various mechanisms have been proposed to describe the formation of the products formed in the Fischer-Tropsch synthesis. The carbide theory (Fischer

and Tropsch, 1926) describes the formation of paraffins and olefins but cannot explain the formation of oxygenated compounds.

The enol condensation (Storch et al., 1951) and the CO insertion mechanism (Pichler and Schulz, 1970) can mechanistically describe the formation of oxygenated compounds. The CO insertion mechanism is the more readily accepted one. Schulz et al. (1990) proposed a combination of the two models.

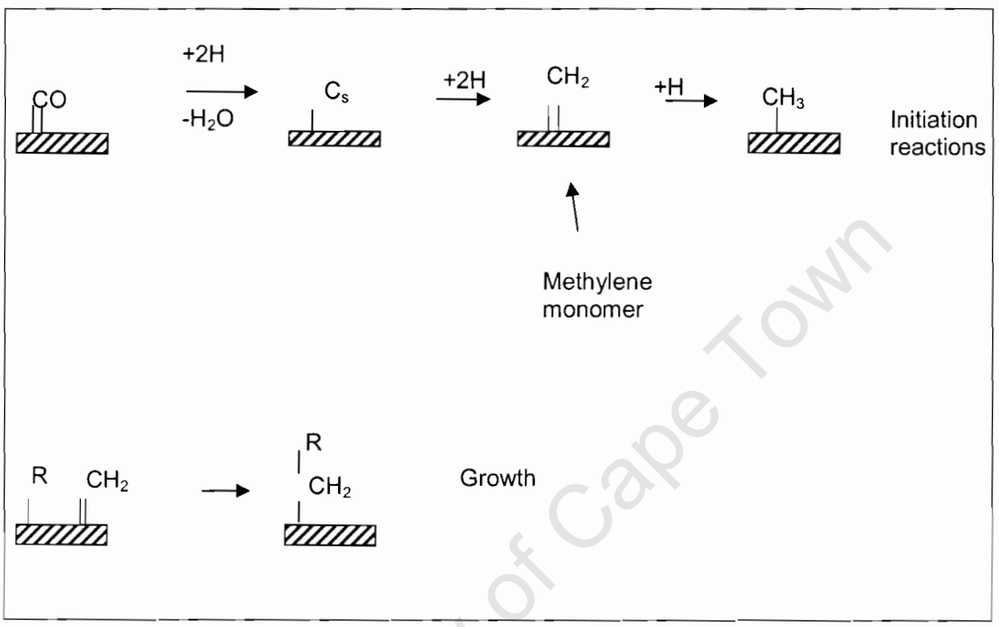


**Figure 1.4:** The Carbide mechanism.

In the carbide mechanism CO adsorbs dissociatively on the catalyst surface and subsequent hydrogenation with adsorbed H leads to methine, methylene and methyl species adsorbed on the surface. The methylene monomer is the surface species mostly involved in further reactions. The incorporation of the methylene monomer into the already formed alkyl species leads to chain growth.

A relatively large amount of alcohols and aldehydes can be formed in the Fischer-Tropsch synthesis. They appear to be primary products. Insertion of some form of oxygenated species is required to account for the formation of these product compounds (Dry, 2002). CO insertion can account for the formation of oxygenated products.

In the CO insertion mechanism CO adsorbs associatively onto the catalyst surface and the incorporation of surface H leads to the formation of oxygenated surface species. The incorporation of alkyl groups into the oxygenated surface specie leads to the formation of aldehydes, alcohols and hydrocarbon species.

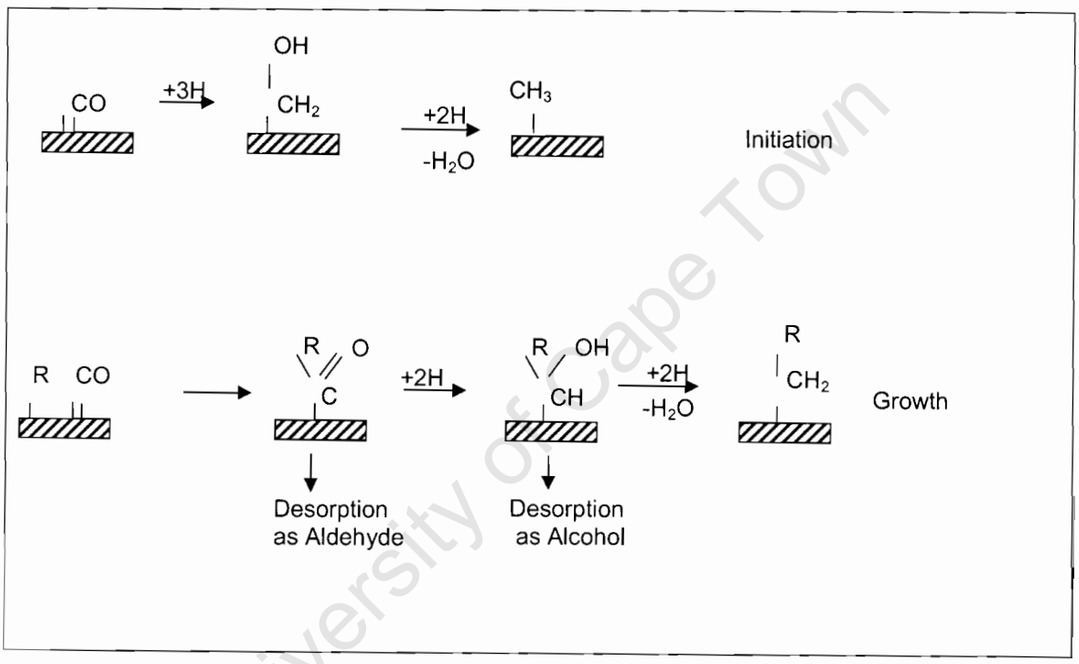


**Figure 1.5:** The CO insertion mechanism.

The adsorbed surface hydrocarbon species formed from either of the proposed mechanisms can undergo desorption at any stage during the chain growth steps, as either a primary olefin or a paraffin.

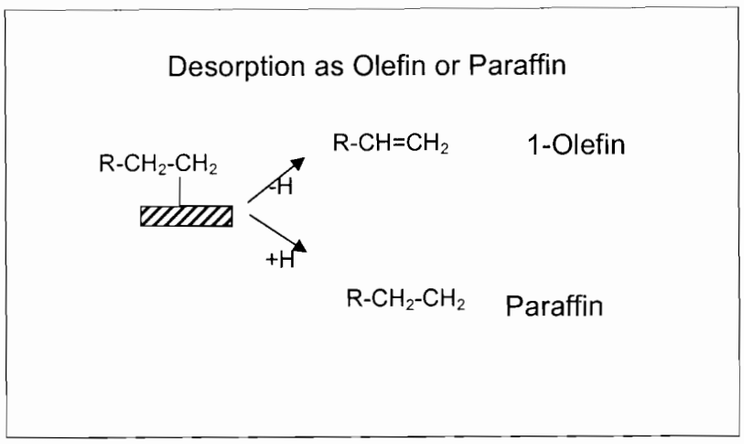


**Figure 1.6:** The desorption steps from the adsorbed alkyl species.

The formed olefin can readsorb onto the catalyst surface due to the double bond of the olefin and can undergo hydrogenation, further growth or desorption as an internal olefin (Schulz et al., 1988).

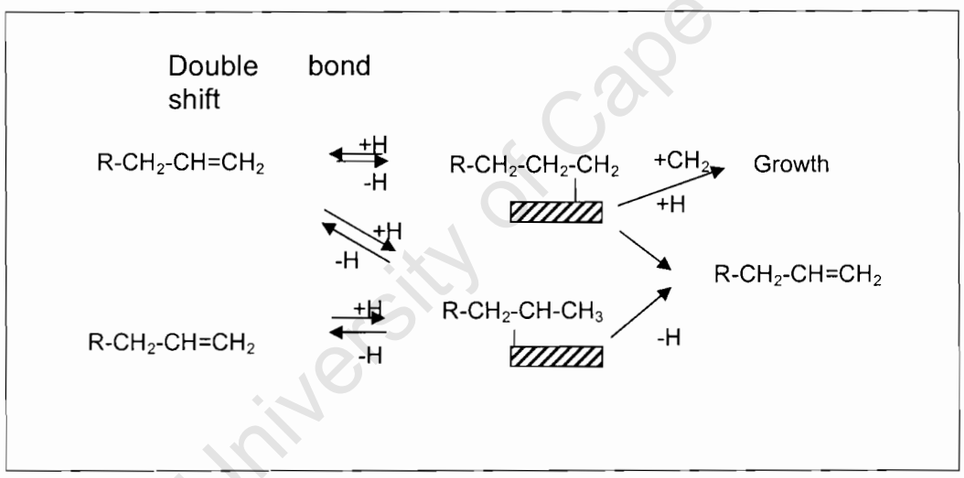


**Figure 1.7:** Secondary reactions of primarily formed 1-olefins.

Primary and secondary branching can occur. Readsorption of olefins from the gaseous phase onto the catalyst surface followed by a branched product being

desorbed is called secondary branching. Primary branching occurs if adsorbed methyl group bonds to the surface methylene carbon, leading to a 2-methyl compound being formed (Schulz et al., 1998).

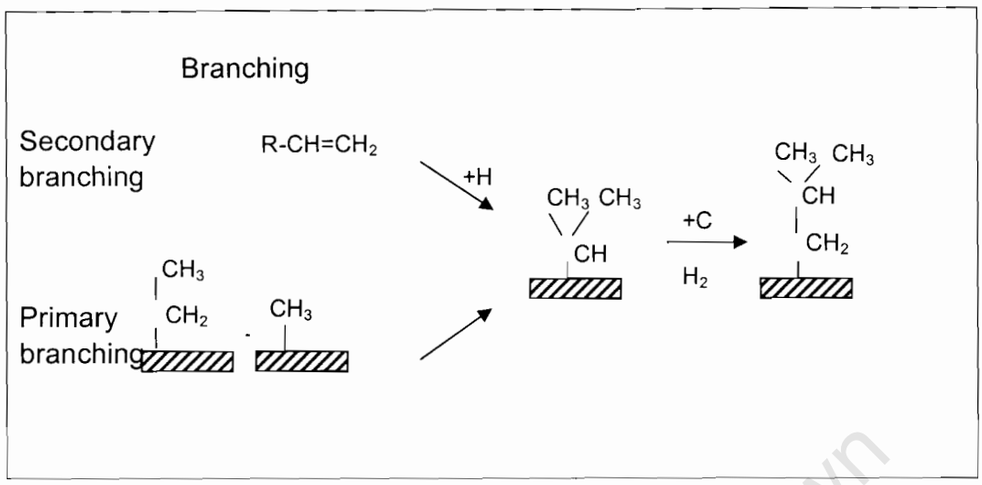


**Figure 1.8:** Reactions leading to the formation of branched products.

The formation of product compounds can be described as a stepwise growth process occurring on the catalyst surface (Dry, 2002). The initiation step starts with the adsorption of CO on the catalyst surface. The chain growth scheme is schematically shown in Figure 1.9 according to the mechanistic steps shown in Figures 1.5-8. At each stage of growth the adsorbed hydrocarbon species can desorb as an alkene or can be hydrogenated and desorb as an alkane, or add another $CH_2$ monomer and to continue the chain growth process.

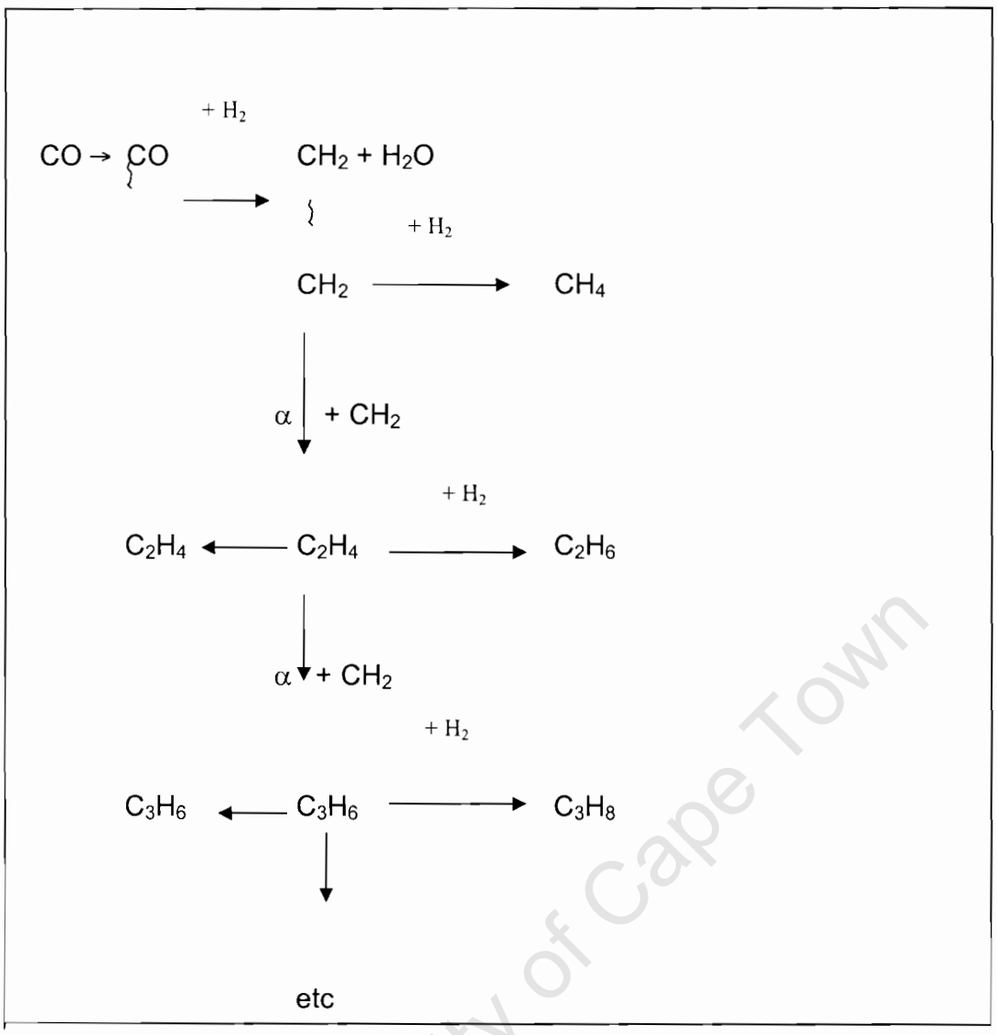


**Figure 1.9:** A schematic of the Fischer-Tropsch stepwise growth process, (no specific mechanism is implied) (Dry, 2002).

The chain growth factor, $\alpha$, gives the probability that the chain growth process will proceed. The probability of chain termination is then given by 1-$\alpha$ (Dry, 2002).

The product spectrum of the Fischer-Tropsch synthesis can be described by the Schulz-Flory distribution (Henrici-Olivé and Olivé, 1976; Dry, 1981).

$$\frac{W_n}{n} = \frac{(1-\alpha)^2 \times \alpha^n}{\alpha} \quad \text{.....(1.8)}$$

Where $W_n$ is the weight fraction, n is the carbon number and $\alpha$ the chain growth probability, which is assumed to be independent of n. The product distribution can be calculated from the value of the chain growth probability factor, $\alpha$ (Dry, 1981).

The Schulz-Flory distribution can be linearised as follows:

$$\text{Log}_e \frac{W_n}{n} = n\text{Log}_e(\alpha) + \text{Log}_e\left(\frac{(1-\alpha)^2}{\alpha}\right) \quad \text{.....(1.9)}$$

A plot of $\text{Log}_e$ ($W_n$/n) against the carbon number, n, gives a graph from which the slope of the straight line can be used to calculate the chain growth probability. The higher the value of $\alpha$ is the more chain growth has occurred and the heavier the product spectrum will be.

Dictor and Bell (1986), and Donnelly and Satterfield (1989), reported that the chain growth probability, $\alpha$, was insensitive to changes in conversion over a wide range of conversions.

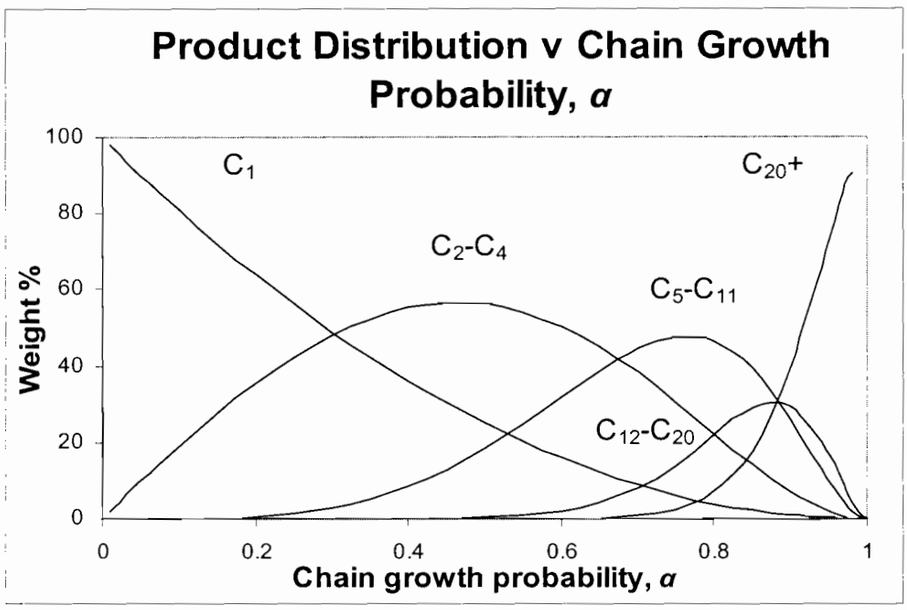


**Figure 1.10:** The product distributions as a function of the chain growth probability, $\alpha$.

### 1.3.2 The Influence of Process Parameters

Typical process parameters that can be varied are temperature, total pressure and partial pressure of feed gas components, space velocity and catalyst composition. The relationship between various process parameters and selectivity of the Fischer-Tropsch reaction has been generalised by Röper (1983). The relationships given in Table 1.1 should only be used as a guideline.

Increasing the $H_2/CO$ ratio leads to a more hydrogenating atmosphere in the reactor. This will lead to more hydrogenated products being formed and a decrease in the chain length (Dictor and Bell, 1986).

**Table 1.1:** Selectivity control in Fischer-Tropsch synthesis by process conditions and catalyst modifications (Röper, 1983).

| Parameter | Chain length | Chain branching | Olefin selectivity | Alcohol selectivity | Carbon deposition | Methane selectivity |
|---|---|---|---|---|---|---|
| Temperature | ↓ | ↑ | * | ↓ | ↑ | ↑ |
| Pressure | ↑ | ↓ | * | ↑ | * | ↓ |
| $H_2/CO$ | ↓ | ↑ | ↓ | ↓ | ↓ | ↑ |
| Conversion | * | * | ↓ | ↓ | ↑ | ↑ |
| Space velocity | * | * | ↑ | ↑ | * | ↓ |
| Alkali content, Fe catalyst | ↑ | ↓ | ↑ | ↑ | ↑ | ↓ |

↑: Increase with increasing parameter

↓: Decrease with increasing parameter

*: Complex relationship

The increase in the olefin and alcohol selectivity with increasing space velocity suggests that they are primary products.

Increasing the alkali content of iron catalysts increases the surface basicity of the catalyst; this leads to an increase in the rate of decomposition of adsorbed CO and increases the rate of free carbon formation. Potassium has been found to increase the rate of carbon formation more than sodium (Dry et al., 1970). The

increase in surface basicity leads to an increase in the chain length of the products formed. It unfortunately also leads to an increase in carboxylic acid formation (Dry, 1981).

## 1.4 CATALYSTS FOR THE FISCHER-TROPSCH SYNTHESIS

### 1.4.1 General Catalysts for Fischer-Tropsch Synthesis

The ability of the group VIII metals to hydrogenate CO increase from left to right across the group. Cobalt, iron and ruthenium are the most active of the group VIII metals for Fischer-Tropsch reaction.

Figure 1.11 shows the rate of methane formation by CO hydrogenation as a function of the heat of adsorption of CO on various group VIII metals (Vannice, 1975). This plot is an example of the so-called volcano plot in which Sabatier's principle is displayed. The intermediate formed on the catalyst surface should be stable enough to form, but not so stable that further reactions do not readily happen. In this example the rate of methanation is the highest for Ru, Co and Fe. The methanation on Cu is very low due to the formation of an associative intermediate compound which then forms methanol.

Ruthenium is a very active Fischer Tropsch catalyst but prohibitively expensive due to its scarcity. At low temperatures and high pressures, > 100 bar, it is very selective towards high molecular waxes (Schulz, 1977). Nickel is a good hydrogenation catalyst but it is very selective towards the formation of methane under Fischer Tropsch conditions. Thus only iron and cobalt are used on an industrial scale (Adesina, 1996).

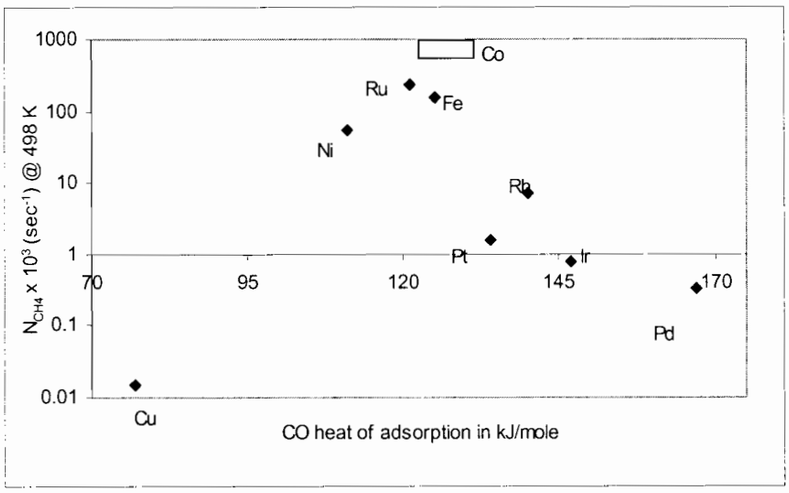


**Figure 1.11:** Rate of methane formation by CO hydrogenation over group VIII metals supported on $SiO_2$ as a function of the heat of adsorption for CO (Vannice, 1975).

Cobalt, due to its high cost relative to iron, is prepared on a support, typically $Al_2O_3$. It is used in the LTFT application to produce long chain linear hydrocarbons. At the higher temperature range of the HTFT process its selectivity towards the methane is too high. Cobalt and ruthenium catalysts display negligible water gas shift activity.

Iron catalysts are commonly used because of their low cost and high availability. They display relatively high water gas shift activity and are used for converting synthesis gas with a low $H_2/CO$ ratio to products. The intrinsic activity of iron is higher than that of cobalt but it deactivates faster (Vannice, 1975). Iron catalysts are used in bulk because of their intrinsic low Fischer-Tropsch reactivity on a mass basis (Sudsakorn et al., 2001). Highly dispersed iron catalysts have also

been found to be difficult to activate by reduction or carburisation (Bukur et al., 1990)

### 1.4.2 Preparation of iron catalysts for the Fischer-Tropsch synthesis

The aim of the catalyst preparation process is to achieve a high surface area in the catalyst precursor, which can result in a large number of catalytically active sites on the surface of the catalyst. Furthermore, large pores are desired to increase rates of mass transfer of reactants and products to the catalytically active sites. Unfortunately catalysts with increased porosity are generally mechanically weaker (Dry, 1981).

Iron catalysts for the Fischer-Tropsch process are commercially prepared either by precipitation or by fusion (Anderson, 1956; Dry, 1981; Dwyer and Hardenbergh, 1983). Novel Fe catalyst preparation techniques, using evaporation or laser pyrolysis, have also been described in literature (Rao et al., 1992). Ultra fine particles prepared by gas evaporation are less than 0.1 μm, are non-porous, and have displayed higher space time yields in slurry reactor tests compared against precipitated iron but separation from product might be problematic. Novel Fe catalysts can be prepared by the laser pyrolysis of organometallic vapour in ethylene, and consist of $Fe_3C$ particles 10-50 nm in diameter. High activity and selectivity towards the formation of light olefins have been observed in some experiments.

#### 1.4.2.1 Precipitation

Iron catalysts are mostly prepared as precipitated catalysts (Anderson, 1956; Dry, 1981). In this process a soluble salt of iron and the precipitant, typically hydroxides, carbonates or ammonia are added together and the precipitate collected. The precipitate must then be separated from the precipitating solution.

The addition of the reagents can be done via continuous precipitation, or batch precipitation (Schüth and Unger, 1997).

Iron salt solutions are acidic due to the following hydrolysis reactions taking place (Schwertmann and Cornell, 2000):

$Fe^{3+} + H_2O \rightarrow FeOH^{2+} + H^+$ .....(1.10)

$2Fe^{3+} + 2H_2O \rightarrow Fe_2(OH)_2^{4+} + 2H^+$ .....(1.11)

$FeOH^{2+} + H^2O \rightarrow FeOOH + 2H^+$ .....(1.12)

$2FeOH^{2+} + H_2O \rightarrow Fe_2O_3 + 4H^+$ .....(1.13)

Large volumes of salt containing solutions are generated during the preparation and must subsequently be removed from the precipitate, usually by washing (Schüth and Unger, 1997).

In the batch-wise precipitation process the one reactant is added stepwise to the other until a predetermined pH is reached. In this case there can be a large difference between the product formed during the initial stages of the precipitation and that towards the end because of pH changes during the precipitation.

In continuous precipitation the reagents are constantly added together at a rate that will keep the pH and temperature of the solutions at a pre-determined level and the formed precipitate is constantly drawn off, or overflows, from the precipitation vessel.

Precipitation consists of three basic steps (Mullin, 1988):

i. The creation of supersaturated solution
ii. Generation of nuclei
iii. Growth of nuclei and agglomeration

The precipitation is started by the rapid mixing of the iron solution and the precipitant resulting in a highly supersaturated system. Nuclei start to form. Due to the low solubility of hydrated iron oxides the rate of nucleation exceeds the rate of growth and a large number of very small particles are generated (Geus, 1986). After an induction period rapid de-saturation starts and the nuclei agglomerate into visible particles. During a ripening phase smaller particles dissolve into the saturated solution and are deposited onto the larger particles.

Ferrihydrite is the initial precipitated product that forms from the fast hydrolysis upon the addition of alkali to a $Fe^{3+}$ salt solution. It is thermodynamically unstable and with time transforms into goethite or hematite or a mixture of the two (Schwertmann and Cornell, 2000).

According to Dry (1981) the pore structure of the catalyst is largely determined by conditions such as temperature, rate of addition and aging that is maintained during the precipitation step. He found that if the alkali solution is added to the iron solution a narrower pore size distribution is obtained. Precipitation at neutral pH values yields a catalyst with a higher surface area.

Motjope et al. (2002) found, by using in-situ Mössbauer spectroscopy, that using $NH_4OH$ as a precipitating agent resulted in the formation of large crystallites of $\alpha$-FeOOH, higher CO conversions and lower olefin selectivities when compared to catalyst that were prepared from either $Na_2CO_3$ and $K_2CO_3$. The carbonate prepared catalysts had smaller crystallites.

Diffenbach and Fauth (1986) investigated the use of sodium carbonate and ammonium hydroxide as precipitating agents, as well as the influence of differing pH upon the synthesis performance of a precipitated iron catalyst. They found an increased olefin to paraffin ratio with a catalyst precipitated with sodium carbonate at a lower pH than that at higher pH or ammonium hydroxide, but the catalyst deactivated quicker.

Iron catalysts prepared by precipitation processes readily undergoes attrition and thermal sintering (Dry, 1981; Pham et al., 2000). In commercial operation this will cause fouling of down stream filters and negatively impact on product quality. To minimise the attrition structural promoters are added (Zhao et al., 2001a; Sudsakorn et al., 2001).

Chemical and or structural promoters can be added during the precipitation step or at a later stage. If $NH_4OH$ is used as the precipitating agent and Cu is a promoter to be added, the Cu should be added after the precipitate is washed free from any residual ammonia due to the solubility of Cu-$NH_3$ complexes.



#### 1.4.2.2 Spray Drying

Spherical particles have superior attrition resistance to precipitated iron catalysts in its as-prepared state (Pham et al., 2000, Reppehagen and Werther, 2000). Spherical particles are obtained by spray drying the collected precipitate. Spray drying is by definition the transformation of feed from a fluid state into a dried particulate form by spraying the feed into a hot drying medium. The form of the final product depends on the physical and chemical properties of the feed and the drier design and operation.

### 1.4.3 Fusion

In the fusion process mill scale from a steel works is fused at about 1770 K, together with a suitable selection of promoters, in an arc furnace and cast into ingots (Dry, 1981; Steynberg et al., 1999). The ingots are cooled, crushed and ball milled to the correct particle size distribution. The surface area of the activated catalyst has been shown to be a direct function of the ratio of $Fe^{3+}$ to twice the amount of $Fe^{2+}$ in the raw material. High surface areas will results in a higher rate of reaction, but unfortunately will lead to a lower mechanical strength in the catalyst particles resulting in the generation of fine catalyst material, which will be lost in the process.

Slow cooling of the molten catalyst will lead to formation of undesirable silicate-inclusions and the non-uniform distribution of promoters in the ingot. The inclusions are rich in alkali promoters and metal oxides (Steynberg et al. 1999). Rapid cooling also limits the growth of large crystals, since the available reaction time at the required temperature is kept short (Schlögl, 1997).



### 1.4.4 Phases Present in Iron Based Catalysts

#### 1.4.4.1 Phases present during activation and synthesis

The activation of iron-based catalysts is done with either $H_2$, CO or a syngas mixture. During the activation the metallic surface area of the catalyst increases (Dry, 1981; Dictor and Bell, 1986; Huang et al., 1993; Shroff et al., 1995).

During activation with hydrogen the hematite is converted into magnetite, $Fe_3O_4$, and elemental iron. Depending on the duration of the reduction with hydrogen, complete conversion to elemental iron, $\alpha$-Fe, can be achieved (Dry, 1981; Shroff

et al., 1995). The reaction steps and thermodynamics that can happen are given as follows:

$3Fe_2O_3 + H_2 \leftrightarrow 2Fe_3O_4 + H_2O$ $\Delta G^{rxn}$( 693K) = -66.7 kJ/mole … (1.14)

$Fe_3O_4 + H_2 \leftrightarrow 3FeO + H_2O$ $\Delta G^{rxn}$( 693K) = +18.9kJ/mole ….. (1.15)

$FeO + H_2 \leftrightarrow Fe + H_2O$ $\Delta G^{rxn}$( 693K) = +9.8 kJ/mole …. (1.16)

$Fe_3O_4 + 4H_2 \leftrightarrow 3Fe + 4H_2O$ $\Delta G^{rxn}$( 693K) = + 48.3 kJ/mole …. (1.17)

From the chemical equations and the Gibbs free energy of reaction (calculated form HSC version 4.0 software ) at 693 K it is clear that it is impossible to reduce hematite further than magnetite using mixtures of hydrogen and water containing less than 50% hydrogen.

Activation with a synthesis gas mixture or CO leads to the partial conversion of $Fe_2O_3$ into $\chi$-$Fe_{2.5}C$ carbide (Bukur et al., 1995). If a synthesis gas mixture is used the temperature of the activation is lower that the synthesis temperature and the temperature is gradually increased as the activation proceeds. It has also been found that catalyst activity initially increased during synthesis time on line and this increase is associated with the conversion of metallic iron and the unreduced iron oxides into ε-$Fe_{2.2}C$ carbide (Bukur et al., 1995). Deactivation was then observed as a result of the inter-conversion of the ε-$Fe_{2.2}C$ into $\chi$-$Fe_{2.5}C$ (Jung and Thomson, 1993).

2.5 ε-$Fe_{2.2}C \rightarrow 2.2\ \chi$-$Fe_{2.5}C + 0.3C$. ……(1.18)

In this conversion reaction amorphous elemental carbon is deposited on the catalyst surface and the authors suggested that it is possible that the deposited carbon can act as nucleation sites for the formation of carbon via the Boudouard reaction.

$2CO \leftrightarrow C + CO_2$ .....(1.19)

The carbides formed are divided into two groups; the O-carbides, with the carbon in octahedral interstices in the iron lattice and the TP carbides, with the carbon atoms in trigonal prismatic interstices. Typical O-carbides are $\epsilon$-$Fe_2C$ and $\acute{\epsilon}$-$Fe_{2.2}C$ and TP carbides are $\chi$-$Fe_{2.5}C$ and $Fe_3C$ (Jung and Thomson, 1993).

The Fischer-Tropsch activity of iron catalysts has been found to be higher when in the reduced form, consisting of magnetite and/or iron metal. Deactivation of iron based Fischer-Tropsch catalysts has thus been associated with the increase in the oxide content of the catalyst (Dry, 1981).

## 1.5 ROLE OF PROMOTERS IN PRECIPITATED IRON CATALYSTS

Promoters are classified as being either structural or chemical depending on the influence that they have on the performance of the catalyst.

### 1.5.1 Chemical Promoters

Iron on its own is not very active towards CO adsorption and dissociation. Adding an alkali promoter such as $K_2O$ increases the strength of CO chemisorption and enhances the dissociation of CO to C and O surface species. The added alkali can also interact with other components in the catalyst such as silica or alumina and it will then unfortunately be rendered less effective. Dry and Oosthuizen (1968) used $CO_2$ chemisorption to study the relative basicities of alkali-promoted reduced magnetite catalyst. They found that for equivalent masses of alkali added to the catalyst the basicity increased in the order Ba, Li, Ca, Na, and K and that higher basicity correlated with a lower selectivity for methane.

Bukur et al. (1990a) found that an increase in the potassium content, from 0.2-1 %m/m, in a precipitated catalyst led to a heavier product spectrum and a decrease in the methane selectivity. A suppression of secondary reactions, such as olefin hydrogenation and isomerisation was also observed.

Increasing the amount of alkali added also increases the rate of carbon deposition (Dry, 1996; Dry, 1981). Dry et al. (1970) studied the formation of carbon on precipitated iron catalyst caused by the decomposition of carbon monoxide (see reaction 1.19). They found that the basic promoters such as sodium and potassium carbonate increased the rate of formation of carbon. However, when the promoters are present as silicates, which are less basic, the rate of carbon deposition is decreased.

Copper is also added as a chemical promoter to lower the temperature at which reduction starts. It thereby reduces sintering and preserves surface area (Dry et al. 1970; Dry, 1981; Dwyer and Hardenbergh, 1984; Bukur et al., 1990a; Dlamini et al., 2002). Bukur et al. (1990a) also observed that copper promotion shifted the hydrocarbon distribution towards heavier products. However, the addition of copper also increased the extent of secondary reactions slightly.



### 1.5.2 Structural Promoters:

Compounds such as $Al_2O_3$, $SiO_2$, $TiO_2$ and group II metal oxides are added to iron catalysts to stabilise high surface areas, preserve pore structure and improve mechanical properties. This is achieved because these compounds act as a physical barrier against the sintering of neighbouring iron-oxide crystallites during calcination or reduction. They are therefore referred to as structural promoters.

## 1.6 ATTRITION

Attrition is defined as the unwanted breakdown of solid particles (British Materials, 1987), which lead to the formation of so-called fines. In the Fischer-Tropsch synthesis fines are regarded as the mass percentage of particles that are less than ca. 22 μm (Jothimurugesan et al., 2000; Sudsakorn et al., 2001; Zhao et al., 2001a and b). Principally, attrition can be attributed to two processes, i.e. chemical attrition and physical attrition.

During activation and Fischer-Tropsch synthesis iron catalysts are subject to both chemical and physical attrition. These two attrition processes lead to the generation of fine catalyst particles, which in commercial processes are usually elutriated or may cause blockages.

### 1.6.1 Physical Attrition

Physical attrition results from collisions between individual catalyst particles and between the particles and the reactor walls and internals. Weak agglomerates from spray dried catalyst particles can fracture into smaller particles. They are abraded under steady state conditions. Abrasion implies that a lot of fines are generated whilst the particle size distribution only slightly shifts towards a smaller distribution (Werther and Xi, 1993; Sudsakorn et al., 2001).

Particle fracture during impact due to pre-existing internal or surface flaws is classified as brittle failure (Zhao et al., 1999) and this process leads to a more pronounced and quicker shift in the particle size distribution towards smaller particles.

#### 1.6.1.1 Fracture

Austin (2002) investigated the impact breakage of particles. He modelled the impact energy of a catalyst particle as being equal to its kinetic energy just before the impact occurs. As the particle hits a surface and is compressed some of the kinetic energy is converted into strain energy. If the minimum energy to cause breakage is exceeded the strain energy is spent in creating new surfaces and heat is released as fragmentation occurs. These fragments still have some kinetic energy and will be compressed and fractured again. This process will continue until all of the originally available impact energy has been converted into strain energy, fracture and heat. Smaller particles require more strain energy to break and are stronger.

#### 1.6.1.2 Abrasion

Cyclone attrition in Fluidised Catalytic Cracking catalyst has been found to be caused by abrasion (Reppehagen and Werther, 2000). The surface energy of the newly created surface has been related by comminution to the kinetic energy that has been spent to create the new surface area. Results also indicate that smaller and spherical particles would undergo less attrition.

### 1.6.2 Chemical Attrition

Chemical attrition can be caused by phase changes, which will result in contraction or expansion of the solid phase. In the iron-based catalysts phase transitions, such as $Fe_2O_3 \rightarrow Fe_3O_4 \rightarrow FeO \rightarrow$ Fe metal $\rightarrow$ Fe carbides, may result in chemical attrition. The conversion of ε-$Fe_{2.2}C$ into $\chi$-$Fe_{2.5}C$, with the formation of elemental carbon (Jung and Thomas, 1993), also leads to chemical attrition. These phase changes cause internal stresses within the catalyst particle and this results in weakening, spalling, or cracking of the catalyst particles (Kalakkad et al., 1995; Shroff et al., 1995; Jothimurugesan et al., 2000). Chemical attrition cause break-up into finely divided catalyst particles, a process that occurs in the nanometre range (Kalakkad et al., 1995).

In the case of fused iron catalyst carbon formation occurs as Fischer-Tropsch synthesis progresses. This carbon will form along the contact zone between inclusions and the iron phase and from the outside to the inside of the catalyst particle (Steynberg et al., 1999). Increasing the amounts of carbon will begin to separate the smaller iron particles from each other within the catalyst particle. This exposes more of the iron particles, and more carbon forms. This then leads to an increase in the size of the catalyst particle and a decrease in the fluidised bed density. The particles also start to break up and the fines content increases. This necessitates the online addition of fresh catalyst.

### 1.6.3 Measuring attrition

Attrition is defined as the unwanted breakdown of solids. The breakdown is quantified by collecting the fines generated, by particle size distribution analysis or by uni-axial compaction (Zhao et al.1999; Pham et al. 1999).

Break-up of catalyst samples can be mimicked in a test in which a sample of the catalyst is impinged against a hard surface. These tests are referred to as collision or drop-shatter tests.

The resistance towards abrasion of catalyst are simulated in fluidised bed tests or jet cup test apparatus. A known mass of sample is fluidised in a tube or vessel with a known gas flow. In these tests the fines elutriated from the bulk of the sample are collected and weighed. This also allows the rate of attrition by abrasion to be determined.

In ultra sonic nebulisation tests the expansion and violent collapse of the generated cavitation bubbles cause intense pressures shock waves in the region of the bubbles. This shock wave interacts with the catalyst particle and then

cause it to undergo erosion or even breakage depending on the strength of the catalyst particle.

In uni-axial compaction a sample is compressed in a cylindrical die and the load at which fracturing occurs gives an indication of the strength of the catalyst.

Werther and Xi (1993) determined the attrition caused by an air jet issuing from an orifice into an already fluidised bed of FCC catalyst. The bed was fluidised by means of a porous gas distribution plate and the jet then impinged into the bed from an orifice. The varied jet velocity was varied from 25 m/s to 100 m/s. Experiments were designed to differentiate between the attrition as caused by the gas bubbles and the air jet. From these experiments they were able to model the attrition rate as being proportional to the jet gas density, the square of the orifice diameter and the cube of the jet exit velocity.

Reppenhagen and Werther (2000) measured the steady state cyclone attrition rate experienced by a FCC catalyst. The abraded fines from the catalyst were collected and weighed. They could model the attrition rate as a function of the square of the cyclone inlet gas velocity and inversely proportional to the square root of the solids/gas loading.

The volume mean moment is used to represent a particular particle size distribution, and is calculated from the particle size distribution itself (Allen, 1997; Zhao et al., 1999; Sudsakorn et al., 2001.). The significance of the volume mean moment is that it is weighted more towards the larger particles and gives an indication of the amount of fracture that catalyst particles have undergone. If the volume mean moment decreases without the amount of fines increasing, fracture of larger particles has occurred without an increase in abrasion.

### 1.6.4 Improving the attrition resistance of a precipitated iron catalyst

Precipitated iron catalyst that contained no structural promoter was characterised by Kalakkad et al. (1995). Their investigation showed that the agglomerates of $FeOOH/Fe_2O_3$ are quite weak and break down readily whilst being analysed by sedigraph analysis for particle size distribution.

Pham and Datye (2000) described silica as providing a morphology that is conducive to creating interlocking forces that holds the iron catalyst together. Bukur et al. (1990a) found that the surface area of an unsupported precipitated iron catalyst was drastically reduced upon calcination and reduction. They ascribed this decrease to the removal of water during dehydration that caused a collapse of the highly porous, high surface area of the $FeOOH/Fe_2O_3$ structure. Introduction of $SiO_2$ into the pores of the precipitate by impregnation with $K_2SiO_3$ provided a rigid matrix that helped to prevent the complete collapse of the original pore structure and thus the surface area of the catalyst is maintained.

Pham and Datye (2000) investigated the role of a silica binder, spray drying and calcination on the attrition resistance of a precipitated iron catalyst with the composition 51 $SiO_2$/9.6 Cu/100 Fe. They found that spray drying and the addition of the silica binder enhanced the attrition resistance of the catalyst significantly. They also found that by first calcining their binder containing catalyst and then spray drying it after re-slurrying led to the best attrition resistance. The catalyst particles formed then were unfortunately irregularly shaped and of a larger particle size. They also had the largest surface area of the range of catalysts and process options tested.

Jothimurugesan et al. (2000) and Zhao et al. (2001a) prepared precipitated iron catalysts adding a $SiO_2$ structural promoter either during the precipitation step or to a re-slurried iron catalyst. In the first instance it is referred to as precipitated

$SiO_2$, and in the latter instance, as binder $SiO_2$. All of the catalysts prepared showed an even distribution of iron and $SiO_2$ throughout the catalyst particle as measured by EDXS analysis. The BET surface areas of the series of catalysts prepared increased almost linearly with the increase in the amount of silica added. In their studies a optimum binder $SiO_2$ concentration of 10-12 % by weight of $SiO_2$ were found to have the highest attrition resistance as measured by the jet cup test. The attrition resistance was measured on samples that were spray dried and then calcined at 300°C for 5 hours. Adding more or less $SiO_2$, or combinations of binder and precipitated $SiO_2$, decreased the attrition resistance. Catalysts that had the highest attrition resistance also had the highest particle density and the lowest macro pore volume. The decrease in the macro pore volume gives an understanding to the observation that the surface area of the samples increased in a linear fashion with an increase in the total $SiO_2$ content. Zhao et al. (2001a) then concluded that particle density plays a major role in governing attrition resistance.

Zhao et al. (2001a) also investigated the influence of a kaolin-clay binder on the attrition resistance and found it to be very readily attrided.

In a subsequent study Zhao et al. (2001b) investigated the effect of carburisation of the catalyst with pure CO at 280°C on the mechanical strength of the particles. Mainly $\chi$-carbide, $Fe_5C_2$ was formed. They found a decrease in the particle size distribution, BET surface area and the volume of the pores less than 10 nm. The particle density of the catalysts increased. These observations are in line with particle shrinkage and pore volume closure. Fracture could only be observed in SEM photos for particles containing less than 10 % silica (binder silica) after carburisation. Particles with more than 10% silica did not show any breakage. Thus, chemical attrition only occurred in the particles with less than 10% silica in the binder form. Based on the particle shrinkage that was observed it would have been suspected that segregation between carbides and the silica framework

would happen. Zhao et al. (2001b) suggested that during the catalyst particle shrinkage that was observed, the silica framework also shrunk.

Sudsakorn et al. (2001) prepared a precipitated iron catalyst containing only precipitated $SiO_2$ in concentrations from 0 to 20 % by weight. The attrition resistance of these catalysts decreased with increasing $SiO_2$ content. The particle density also decreased with an increase in the $SiO_2$ concentration. The authors then concluded that the concentration rather than the point of addition of $SiO_2$ govern the attrition resistance and they corroborated the relationship between particle density and attrition resistance.

Pham and Datye (2000) measured the attrition resistance of a precipitated iron catalyst prepared with and without a $SiO_2$ binder by using ultrasonic nebulisation. They found that the inclusion of the binder greatly enhanced the attrition resistance as measured by the absence of particles less than 5 μm after 25 minutes of ultrasonic irradiation.



## 1.7 INFLUENCE OF BINDER ON ACTIVITY AND SELECTIVITY

Egiebor and Cooper (1985) studied the synthesis performance of a precipitated iron catalyst containing 4.7 K/2.9 Cu/x $SiO_2$/100 Fe (x= 21,50,73). Silica was added as a binder. The catalysts were evaluated for the activity in the Fischer-Tropsch synthesis at 300° C, 7 bar, a gas hourly space velocity of 240 v/v $h^{-1}$, and a $H_2$/CO ratio of 1. Their study showed a relatively constant CO conversion and total paraffin and olefin selectivity with an increase in the $SiO_2$ concentration. An increase in the selectivity towards n-alkanes was observed, the 1-olefin selectivity also increased but less than that of the n-alkanes, thus resulting in a decrease in the 1-olefin to n-alkane ratio. A decrease in the branched hydrocarbon selectivity and an increase in the internal olefin selectivity were observed with an increase in the silica concentration. The alcohol selectivity

remained constant. They suggested that strong-metal support interactions could be a cause for their observations.

These observations do not follow the same trend as that predicted by Table 1.1. Strong –metal support interactions would be expected to decrease the effective potassium content in the catalysts with an increase in the support concentration. According to Table 1.1 this should lead towards a lighter product spectrum, an increase in chain branching, a decrease in olefin selectivity and a decrease in alcohol selectivity. No explanation for these deviations is given.

Bukur et al. (1990) compared the activities and selectivities of precipitated iron catalysts containing none and varying amounts of structural promoters. The structural promoters were added in the binder form. The catalyst composition was 4.2 K/5 Cu/ x $SiO_2$/100 Fe (x = 8,24,100) and 4.2 K/5 Cu/x $Al_2O_3$/100 Fe (x= 8,24). The catalytic activity in the Fischer-Tropsch synthesis was evaluated in a fixed bed reactor at 225 °C, 15 bar, a gas hourly space velocity of 2 $l_N/(g_{cat}.h)$, and a $H_2$/CO ratio of 1.0. They found that the Fischer-Tropsch activity and the water gas shift activity declined with an increase in the structural promoter concentration. The authors ascribed this to interactions between potassium and/or iron with the supports.

On the catalyst containing 8 $SiO_2$/100 Fe the $C_1$-$C_{11}$ selectivities were generally lower and the $C_{12}$+ selectivity higher than those obtained on the catalyst containing no structural promoter. Levels of binder $SiO_2$ at 24 and 100 /100Fe showed a marked decrease in activity and a shift towards both $CH_4$ and $C_{12}$+ selectivities.

A decrease in the selectivity towards total olefins and an increase towards 2-olefin selectivity was observed, the decrease became more pronounced with an increase in the carbon number and an increase in the amount of silica used. Dictor and Bell (1986) and Bukur et al. (1990 (a)) observed that with an increase

in the potassium content of a precipitated iron catalyst a decrease in olefin hydrogenation and isomerisation was obtained.

These observations are in line with the argument that an increase in the structural promoter concentration lead to an increase in the metal support interaction and then decreasing the effective potassium concentration in the catalyst.

The catalysts containing 8 and 24 $Al_2O_3$/100Fe displayed lower conversions compared to the catalysts containing the same amount of binder $SiO_2$/100Fe. The lower conversions can be ascribed to a stronger interaction between the alkali promoter and the more acidic structural promoter, $Al_2O_3$.

Jothimurugesan et al. (2000) compared the activity and selectivity of a precipitated iron catalyst, containing binder and precipitated silica, with a Ruhrchemie standard catalyst. The Ruhrchemie standard catalyst had the following composition: 100Fe/5Cu/4.2K/25$SiO_2$. The silica was added in the precipitated form. The precipitated catalyst was prepared to contain the same amount of copper and potassium as the standard Ruhrchemie catalyst. The silica binder/precipitate concentration was varied. The precipitated $SiO_2$ catalyst was prepared with a binder $SiO_2$ content of 10%. They compared the synthesis performance in a fixed bed micro reactor at 270°C, 14.8 bar and a $H_2$/CO ratio of 0.67. For the catalyst with the optimum attrition resistance, a binder concentration of 12 %, they found a higher activity; 94 % CO conversion versus 86 %, slightly lower $CH_4$, $C_2$-$C_4$ and $C_5$-$C_{11}$ selectivities and a higher $C_{12}$+ selectivity than the standard catalyst (containing 18 % binder silica). Their results indicate that an increase in the structural promoter concentration led towards an increase in the selectivity for $C_1$-$C_{11}$ products and a decrease in the $C_{12}$ selectivity.

## 1.8 HYPOTHESIS STATEMENT

The concentration of the structural promoter determines the attrition resistance of the catalyst. Attrition resistance can be achieved using by the addition of low levels of structural promoter during the precipitating of the iron catalyst. At structural promoter concentrations of less than ca. 10g/100g Fe the changes in activity and selectivity are expected to only be a function of the chemical promoter concentration.

# 2 EXPERIMENTAL PROCEDURES

## 2.1 Catalyst preparation

The catalysts used in this study were all prepared by continuous precipitation using iron nitrate as the Fe source and ammonium hydroxide as the precipitating agent. The precipitate was subsequently dried to a filter cake in a filter press. The chemical promoters were added. The catalyst precursor was subsequently spray-dried and calcined.

Aluminium nitrate was added as the structural promoter and as a possible attrition resistance enhancement promoter. Sodium, copper and chromium were added as chemical promoters. The aluminium can also act as a chemical promoter because of its ability to affect activity and selectivity.

Two series of catalysts were prepared. In the one series the aluminium nitrate salt was added to the Fe solution prior to the precipitation step, and in the other series the aluminium nitrate was added to the re-slurried filter cake. The chemical promoters were added to the catalysts just before the spray-drying step. In addition to these catalysts, a catalyst without aluminium addition was prepared. The composition of the prepared catalysts is given in Table 2.1.

The nomenclature used in this thesis will be as follows: the samples with the $Al_2O_3$ added during the precipitation step will be referred to as the "**P**" series samples and those with the $Al_2O_3$ added to a re-slurried filter cake as the "**B**" series samples. The sample with no $Al_2O_3$ added will be referred to as "**N**". **P(0.5)** is then the sample with 0.5 $Al_2O_3$/100 Fe added during the precipitation step.



### 2.1.1 Precipitation

The catalysts were prepared by continuous precipitation from the metal salt solution using a 25 % (m/m) aqueous ammonia solution as the precipitation agent (see Figure 2.1). The metal salt solution was prepared by dissolving 3.40 kg of analytically pure iron nitrate, $Fe(NO_3)_3.9H_2O$, in deionised water at

**Table 2.1**: Mass of promoter salt weighed out per 1.00 kg of Fe.

| Salt | Molecular mass, g/mole | Mass of Salt (g) | Promoter | Calculated promoter (g) per 100g Fe | Nomenclature used |
|---|---|---|---|---|---|
| $NaNO_3$ | 85.0 | 5.49 | $Na_2O$ | 0.2 | |
| $Cu(NO_3)_2.3H_2O$ | 241.6 | 26.3 | Cu | 0.5 | |
| $Cr(NO_3)_3.9H_2O$ | 400.1 | 23.1 | Cr | 0.3 | |
| | | | | | |
| | | | | $Al_2O_3$: | |
| $Al(NO_3)_3.9H_2O$: | 375.14 | 0 | | 0.0 | N |
| | | 14.7 | | 0.2 | |
| | | 36.8 | | 0.5 | P(0.5), B(0.5) |
| | | 73.6 | | 1.0 | P(1.0), B(1.0) |
| | | 110.4 | | 1.5 | P(1.5) |

room temperature and diluted to 10 litre in a plastic container. This gave a solution containing 60 grams Fe per litre. For the series of catalysts in which the aluminium nitrate was added during the precipitation step the required amount of aluminium nitrate (see Table 2.1), was weighed off and added to the iron nitrate prior to the addition of the deionised water. The metal salt solution and the aqueous ammonia solution were pumped into the precipitation vessel using peristaltic pumps.

The pH of the precipitating solution was measured using a pH electrode. It was placed in the precipitation vessel close to the side of the vessel but not so close that the slurry could not pass between the electrode and the vessel sides. The pH electrode was calibrated with commercial pH buffer tablets of pH 4.2 and 7.0 prior to the precipitation.

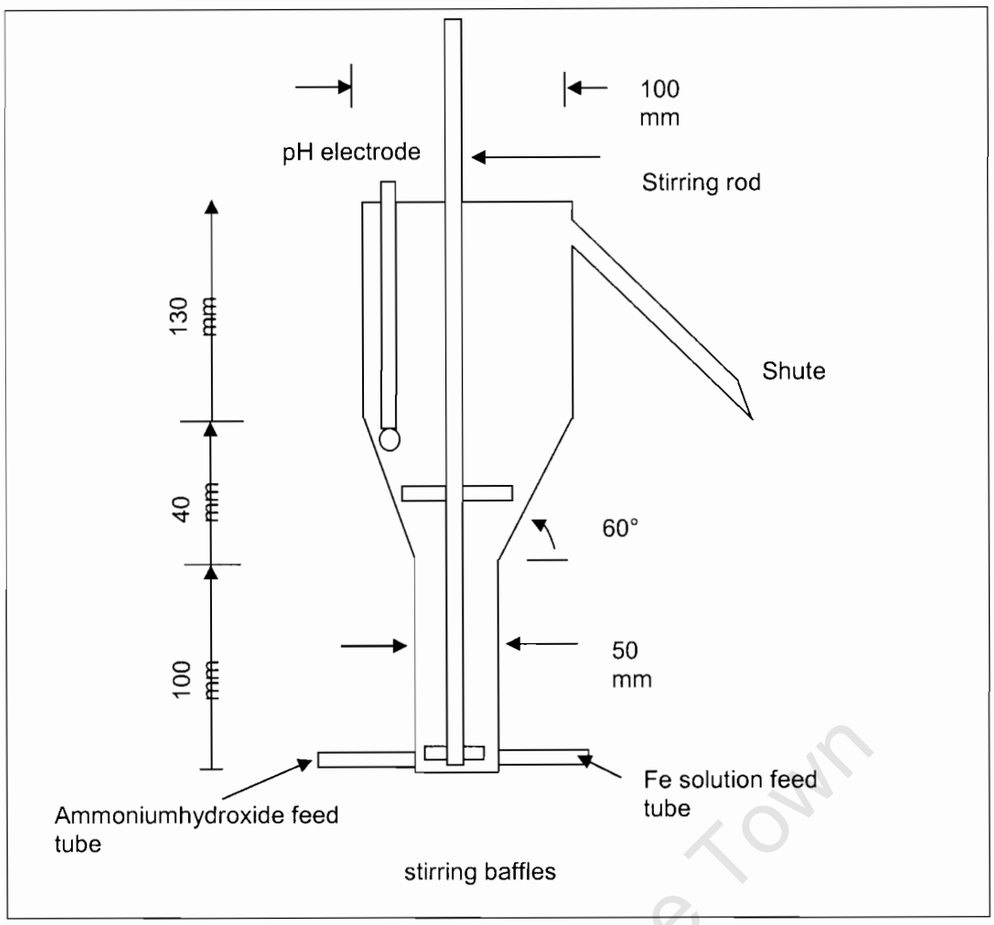


**Figure 2.1**: A schematic of the precipitation vessel used. The measurements are only approximate.



The precipitation solution was stirred with an overhead stirrer at a speed of ~ 1500 rpm. The stirring rod of the overhead stirrer was placed as far as possible into the precipitation vessel, with the impeller as close as possible to the inlet of the iron solution and the precipitating agent.

The peristaltic pumps were initially set to deliver a loading of reagents to the continuous precipitation vessel of ~ 35 % for the ammonium hydroxide and 100 % for the iron nitrate solution. This setting was then fine-tuned to maintain the pH between 7.3 and 7.8 during the precipitation. The slurry produced from the precipitation vessel was discarded until the correct pH range was

achieved. The temperature during the precipitation was maintained between 28°C and 32 °C.

### 2.1.2 Filtering and Washing of the Precipitate

The slurry that was collected from the precipitation vessel was filtered through a filter press and washed free of any nitrate and hydroxide salts with deionised water until the wash water had a conductivity of < 120 µS. During filtering, the wash water feed was periodically stopped and instrument air forced through the filter press in order to force out any water collected in regions where there was an inadequate flow of wash-water. This minimised the effect of the wash-water channelling through the formed filter cake.

A relatively dry filter cake was obtained which typically contained ~ 85 % solids as measured by heating to a constant weight at 150°C. The filter cake was then stored in sealed plastic buckets.

The Fe content of the filter cake was determined by the $K_2Cr_2O_7$ titration, see section 2.2.1.1. The so determined amount of iron in the catalyst precursor was used to calculate the quantity of promoters that had to be added.

### 2.1.3 Re-slurrying and Promoter Addition

Approximately 5 kg of the filter cake was weighed out into a 10 litre plastic bucket. The appropriate mass of promoter salts was weighed out (see Table 2.1) to the nearest 0.01g. The promoter salts were then dissolved in the least amount of deionised water and quantitatively added to the slurry. The slurry was then homogenised with an overhead stirrer and small amounts of deionised water added until the solids content decreased to ca.12% for the spray drying.

### 2.1.4 Spray Drying and Calcination

Spherical particles have superior attrition resistance (Reppehagen and Werther, 2000). To get spherical particles the collected precipitate is spray dried. Spray drying is by definition the transformation of feed from a fluid state

into a dried particulate form by spraying the feed into a hot drying medium. Spray drying consists of four process steps, which happen consecutively:

1) Nebulisation of the feed into a spray
2) Spray-air (drying medium) contact
3) Drying of the formed spray
4) Separation of the dried product from the air

Centrifugal, pressure or sonic effects provide the energy for the nebulisation process. Evaporation is promoted by spraying the feed into a heated atmosphere as small droplets. The evaporation takes place from the saturated vapour film that is established at the droplet surface. The temperature at the droplet surface approximates that of the wet bulb temperature of the drying air.

The evaporation takes place in two stages. During the first stage there is enough moisture within the droplet to replenish that lost at the surface. Diffusion of moisture from within the droplet maintains saturated surface conditions. This stage is generally referred to as the constant rate of cooling period. When the moisture becomes to low to maintain the saturated conditions the so-called critical period is reached and a dried shell is formed at the surface. Evaporation is then dependent on the rate of moisture diffusion through the dried surface shell.

If the available nebulisation energy is held constant but the feed rate is increased, sprays with a larger droplet size will result. Increases in viscosity and surface tension for the same amount of nebulisation energy will also result in larger droplet sizes.

The promoter-impregnated slurry was fed into a mixed flow spray drier (see Figure 2.2). A TX 2.5 mm Unijet Hollow cone nozzle tip was used for nebulisation. The slurry was fed to the spray drier using a Hydra-cell G-13 positive displacement diaphragm feed pump. The spray-drying conditions are given in Table 2.2.

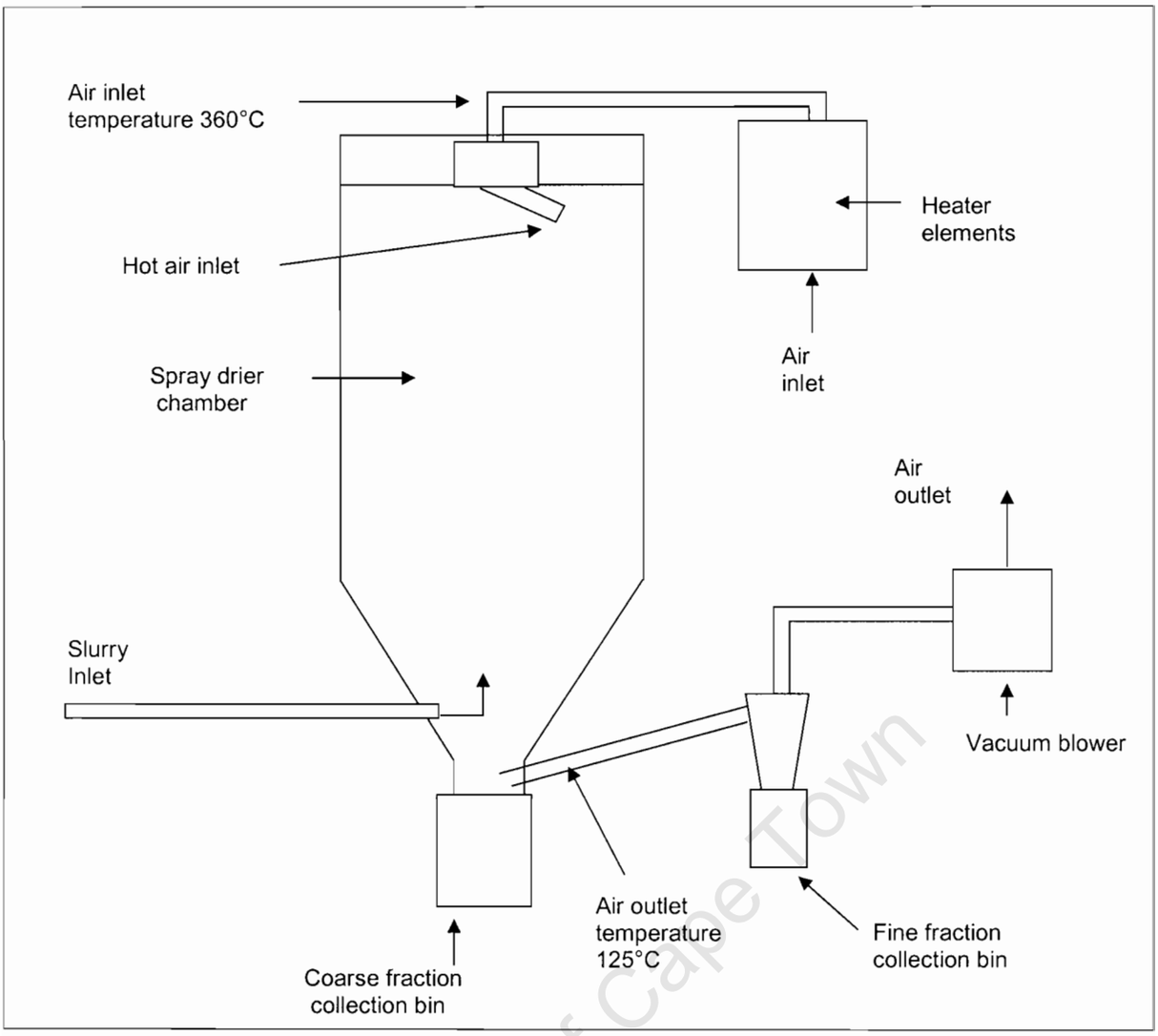


**Figure 2.2:** Schematic of spray drier used.

**Table 2.2:** Conditions for spray drying of the re-slurried precipitate.

| | |
|---|---|
| Slurry feed rate, litre/hr | ca. 20 |
| Slurry delivery pressure, bar | 15 |
| Solid content in slurry, wt.-% | ca. 12 |
| Nebuliser | TX 2.5 mm Unijet Hollow cone nozzle tip |
| Inlet temperature air, °C | 360 |
| Outlet temperature air, °C | 125 |

The first fractions from both the collection bins were discarded. The fine and coarse fractions were then combined as a final product.

The spray-dried catalyst was subsequently calcined at 350 °C for 4 hours in an air atmosphere. The calcination oven was ramped to 350°C at a rate of 2°C per minute. The catalysts were placed in a flat pan with a bed thickness not exceeding 3-4 mm. Any residual nitrates present in the catalyst samples will decompose at this temperature.

## 2.2 CHEMICAL CHARACTERISATION

### 2.2.1 Chemical Composition

#### 2.2.1.1 Total Iron Concentration

The iron content of the samples was determined by the standard Potassium-dichromate redox titration method. A mass of sample is dissolved in a 1:1 HCl acid solution, the $Fe^{3+}$ in the acid solution is reduced to $Fe^{2+}$ with $SnCl_2$ in a strong acidic solution. The residual $Sn^{2+}$ is reduced to $Sn^0$ with $HgCl_2$. The sample solution is then kept in an inert atmosphere by the addition of dry ice. The $Fe^{2+}$ in the sample is then titrated with a 0.008M $K_2Cr_2O_7$ solution with NDAS as the indicator. As the $Fe^{2+}$ is consumed the excess $Cr^{6+}$ causes the indicator to turn green. The endpoint is taken when the indicator changes to green.

#### 2.2.1.2 Promoter Concentration

The promoter concentration of the catalysts prepared was determined by ICP-AES. A mass of sample that contained 0.1 g of iron was weighed off to the nearest 0.1 mg, and then dissolved in 40 ml of 1:1 HCl mixture by boiling under reflux. The resultant sample solution was transferred quantitatively to a 100 ml volumetric flask and diluted to 100 ml with de-ionised water. The standards used were prepared such that they contain the same amount of iron as the samples did.

The ICP-AES used was a Varian model sequential instrument. The Nebuliser was of a glass concentric design and a PTFE spray chamber was used. The

ICP torch was a normal glass torch. The RF source was a 40 MHz source and the instrument was set at a forward power of 1.3 kW.

**Table 2.3:** The analytical lines used for the ICP.

| Analyte | Wavelength used |
|---|---|
| Na | 588.9 nm |
| Cu | 324.8 nm |
| Cr | 206.1 nm |
| Al | 396.1 nm |

The concentration of the analyte per 100 gram of iron ($m_i$) was calculated as follows;

$$m_i = \frac{(I_{sample} - I_{blank})}{(I_{standard} - I_{blank})} \times Std \times \frac{100\,ml}{1000\,ml/l} \times \frac{1}{m} \times \frac{100\%}{\%\,Fe} \times \frac{100\,Fe}{1} \quad .....(2.1)$$

$I_i$ : Intensity measured of sample, standard or blank.

Std : Analyte standard concentration in mg/l

m : mass of sample used in g

## 2.3 Catalyst Morphology

### 2.3.1 Surface Area Analysis

The surface area analysis was determined using the physiosorption of nitrogen on a Micromeritics Tristar. The strength of the physical adsorption of gases by solids increases with a decrease in temperature and an increase in pressure. The equation used for the relationship between the amount of gas adsorbed and the total surface area of the solid is commonly known as the BET equation.

$$\frac{\frac{P}{P_0}}{\left(V_a\left(1-\frac{P}{P_0}\right)\right)} = \frac{1}{V_m C} + \frac{(C-1)}{V_m C} \times \frac{P}{P_0} \quad \text{.....(2.2)}$$

Where:

$P_0$ : Saturation pressure of the gas used

P : Pressure at measurement point

$V_a$ :Quantity of gas asdsorbed at pressure P

$V_m$ :Quantity of gas adsorbed when entire surface is covered with monolayer

C :Constant

A plot of $P/(V_a(P_0-P))$ versus $P/P_0$ should yield a straight line with intercept $1/(V_mC)$ and slope $(C-1)/(V_mC)$ and from the volume of the monolayer the surface area can be calculated assuming that the area of a $N_2$ molecule is 16.2 $Å^2$.

### 2.3.2 SEM Characterisation

The morphology of the catalyst particles was examined using scanning electron microscopy (SEM). A LEO 1413 instrument was used and it was coupled to a i-XRF-EDS system. The images were taken by secondary electron emission.

### 2.3.3 Crystallographic Phase Analysis

The phases present in the catalyst were determined using XRD. A Siemens Kristalloflex instrument was used in conjunction with a Co K-$\alpha$ source. The catalyst powder was pressed in a plate with a ~ 2 cm wide recess being 2 mm deep. The analysis was started at an angle of $2\theta$=5° and stopped at an angle of $2\theta$=95°. The step time was set at 3 seconds per step with a scanning angle of 0.02° per second.

Quantification of the XRD-spectrum was done with a Siroquant version 2.0 software package. The crystallite diameter was determined from the Scherrer

equation (equation 2.3). The peak width was corrected for the instrumental broadening of the peak width, which was determined by recording the XRD spectrum of NaCl.

$$\langle L \rangle = \frac{K.\lambda}{\beta.\cos\left(\frac{2\theta}{2}\right)} \quad \text{.....(2.3)}$$

K: Constant, taken as 0.9 for peak width at half peak height.

$2\theta$: Angular position of peak maximum

$\lambda$: Wavelength from source, for Co it is 1.78897 Å

$\beta$: Corrected peak width at half peak height, expressed in radians

L: crystallite diameter in units of source wavelength

The peak width at half peak height was determined graphically from the XRD spectra by importing it into Excel. The baseline was obtained by selecting a point on each of the baseline shoulders and extrapolating. The spectra were smoothed by selecting a 10 point moving average.

## 2.4 Physical Characterisation

### 2.4.1 Density Measurements

The density of a material is defined as its mass divided by its volume. The type of volume measurement made on the material defines the type of density that is calculated.

#### 2.4.1.2 Absolute density

The absolute density or the skeletal density is obtained when the volume measurement excludes the volume of the pores in the material as well as the inter-particle void volume. This density measurement is typical made by using He as an intrusion gas. Therefore, this density is commonly referred to as He

density. The skeletal densities of the catalysts were determined by He intrusion.

### 2.4.1.3 Particle and Bulk Density

The particle or envelope density is the density reported when the volume measurement includes the volume of the pores within the particle but excludes the volume caused by inter-particle voids. This density can be calculated from the pore volume of the sample and the absolute density.

The particle density can also be obtained from mercury intrusion porosimetry, MIP, measurements. In the MIP analysis Hg is forced against its surface tension into progressively narrower pores as the applied pressure is increased. There is an inverse relation between the pressure applied and the pore diameter, the relationship is quantified by the Washburn Equation:

$$\text{Washburn equation}: D = \frac{4\gamma(\cos\theta)}{P} \quad \text{.....(2.4)}$$

where

$\gamma$ = surface tension in $N.m^{-1}$
$\theta$ = contact angle
P = pressure applied in kPa

The contact angle, advancing and retracting, was taken as 130° and the surface tension of the Hg as 0.485 $N.m^{-1}$. The diameter is reported in meter.
The bulk density of a material is the density calculated when the volume measurement includes the pore volume and the inter-particle void volume. It is not an inherent property of the material but depends on the particle shape.

The following samples were analysed for their particle and bulk density by MIP: **N**, **P(1.0)** and **B(1.0)**.

### 2.4.2 Temperature Programmed Reduction

A Micromeritics Autochem 2910 Temperature Programmed Reduction, TPR, instrument was used to performed TPR analysis on selected catalysts in order to determine the amount of reducible species in the catalyst, and the temperature at which these species are reduced. Approximately 0.05 g of sample was accurately weighed out into a quartz U-tube. A helium flow was passed over the sample at a temperature of 120°C to dry the sample. The temperature programmed reduction was performed with 10% $H_2$ in argon gas stream at a flow rate of 50 $ml_N$/min. The sample was heated at a rate of 10°C per minute up to a final temperature of 900°C. The concentration of hydrogen in the effluent was measured using a TCD. The effluent passed through a Dewar containing a dry-ice and an acetone mixture prior to entering the TCD to condense any water in the carrier gas line to the TCD detector. The presence of water in the gas to the TCD detector will influence the signal.

### 2.4.3 Particle Size Distribution

The particle size distribution of the catalyst particles was determined by light scattering measured from a laser (see Figure 2.3). In this technique the particles of interest are irradiated by electromagnetic radiation of a given wavelength. Each of the particles then acts as a scattering centre because of the diffraction of the light from the edges of the particle. The angle of diffraction is inversely proportional to the size of the particle. The resulting light intensity as a function of the angle of diffraction is analysed mathematically to determine the particle size distribution.

Either the Mie or the Fraunhöfer theory is used to de-convolute the signal. In the Mie theory the effects of the light undergoing refraction through the particles and the absorbtion of the particles are taken into account. The Fraunhöfer theory is based only on the diffraction of light around the particles and its application is limited to particles larger than ~20μm. The Mie theory accounts for all particle sizes and was used to report the particle size distribution of the catalysts analysed.

The particle size distribution was determined with a Micromeritcs Saturn Digisizer laser diffraction instrument fitted with a CCD detector. Samples were

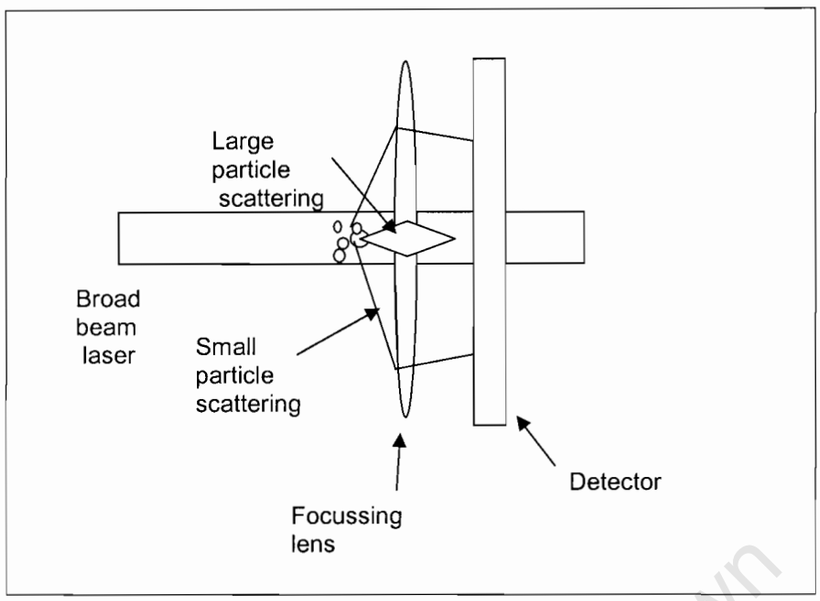


**Figure 2.3**: A schematic of the particle size measurement by light scattering instrumental principle.

well dispersed with 1ml of a sodium hexa-metapolyphosphate (10 g/litre) solution in a spatula and then introduced into the sample compartment of the instrument. The analysis liquid used was ethanol ($\eta$ = 1.003 cP, $\rho$ = 0.791 g/cm$^3$). The operation conditions are given in Table 2.4. Each measurement was repeated three times. The volume percentage distribution of the particles as a function of the equivalent diameter is reported.

**Table 2.4:** Conditions for determining the particle size distribution

| | |
|---|---|
| Instrument | Micromeritcs Saturn Digisizer |
| Detector | CCD |
| Liquid | Ethanol |
| Liquid flow rate | 12 litre/min |
| Circulating time | 200 seconds |
| Beam angle | Up to 45$^o$ |

## 2.5 Measuring the attrition resistance of the catalysts prepared

The resistance towards impact attrition of the catalysts were determined by jet impingement analysis. The catalyst samples are impinged against a metal plate and the shift towards a finer particle size distribution measured.

### 2.5.1 The Jet Impingement equipment

The jet impingement equipment used to measure the attrition resistance of the catalyst particles is shown Figure 2.4. The sample is loaded in the sample conveying tube. Upon opening the solenoid valve, the sample is accelerated along the sample conveying tube and impinged on the plate at the outlet. After the entire sample has settled into the sample receiver it is removed from the receiver flask and then analysed for its particle size distribution.

The chamber of the solenoid controlled release valve has a volume of 10 ml and it is pressurised to 0.7 MPa before the pressure is released.

The sample conveying tube is a 1/4-inch stainless steel tube with an internal diameter of 4.5 mm. The sample conveying tube is connected to the outlet of the solenoid valve. The total length of the tube is 45 cm and the impingement plate is situated 3 cm from the outlet of the tube.
The radius of curvature is approximately 2 cm. The sample receiver is a 5 litre Erlenmeyer flask. A sample mass of 0.5 g is inserted into the sample conveying tube and once connected the pressure is released.

In order to evaluate the actual material strength of the catalyst particles the catalyst is sieved to a specific particle size fraction. This is done to minimise the influence of particle size distribution between various catalysts.

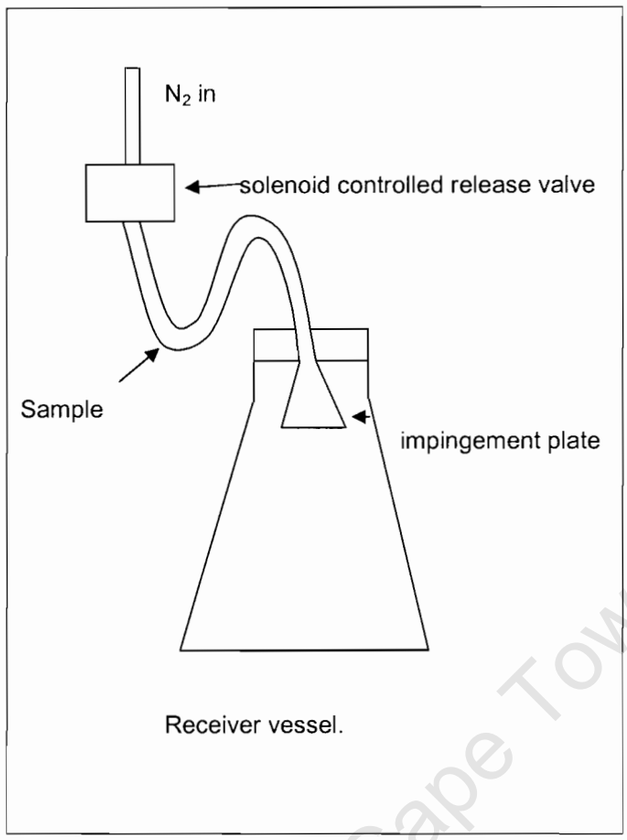


**Figure 2.4:** A schematic of the Jet Impingement apparatus.



It is to be expected (Repenhagen and Werther, 2000) that catalysts with a particle size distribution shifted towards smaller particles would be more resistant to impact attrition. In the Jet Impingement analysis the mass of catalyst loaded into the apparatus is held constant. This means that for catalysts with a particle size distribution towards larger particles, fewer particles will be loaded and that the "cushioning effect" of other particles impinging prior to any specific particle will be less. If fine particles are present the number of particles loaded will be more and an increase in the "cushioning effect" might be observed. A change from "brittle to plastic" behaviour is also

observed with a decrease in particle size distribution (Hess and Schönert, 1981).

In the case of samples being sieved prior to Jet Impingement the difference between the mean of the particle size of the sample, prior to impingement, to that after Jet Impingement can be used as a single value parameter to describe the resistance to attrition. This is termed the Breakage Index and is calculated as follows:

Breakage Index, BI,

$$= \frac{(\text{Mean particle size before JI} - \text{Mean particle size after JI})}{\text{Mean particle size before JI}} \times 100 \quad \text{.....(2.5)}$$

For the catalysts selected the particle size fraction chosen was between 38 and 63 μm. This range was based in the commercially available sieve sizes and the fact that it seems to include the middle third of the particle size range of the original catalysts.

## 2.6 Catalyst evaluation in the Fischer-Tropsch Synthesis

The Fischer-Tropsch catalytic activity and selectivity of selected catalysts was investigated using a Berty micro reactor (see Figure 2.5). The Berty micro reactor has a high internal recycle and is considered to approximate a continuous stirred tank reactor, CSTR.

The catalyst is supported on woven gauze stuck on a metal mesh, with the woven gauze having ~ 12 μm pores. The diameter of the insert, on which the catalyst rests, is 70 mm (surface area=38.5 $cm^2$). The layer of catalyst is covered with a piece of glass wool to keep it in place.

The impeller vanes cause a slight vacuum underneath the gauze and this sucks reacting gases through the gauze. The gas flow in the reactor is then

upwards from the impeller up the annular space and then down and through the catalyst bed.

### 2.6.1 Operating Conditions

The reactor operating conditions that were used for the reactor runs are given in the Table 2.3. The pressure in the reactor is maintained at the set value by using a backpressure regulator. The feed gas composition was controlled by mass flow controllers to be as given in table 2.5. The Ar is added as an internal standard.

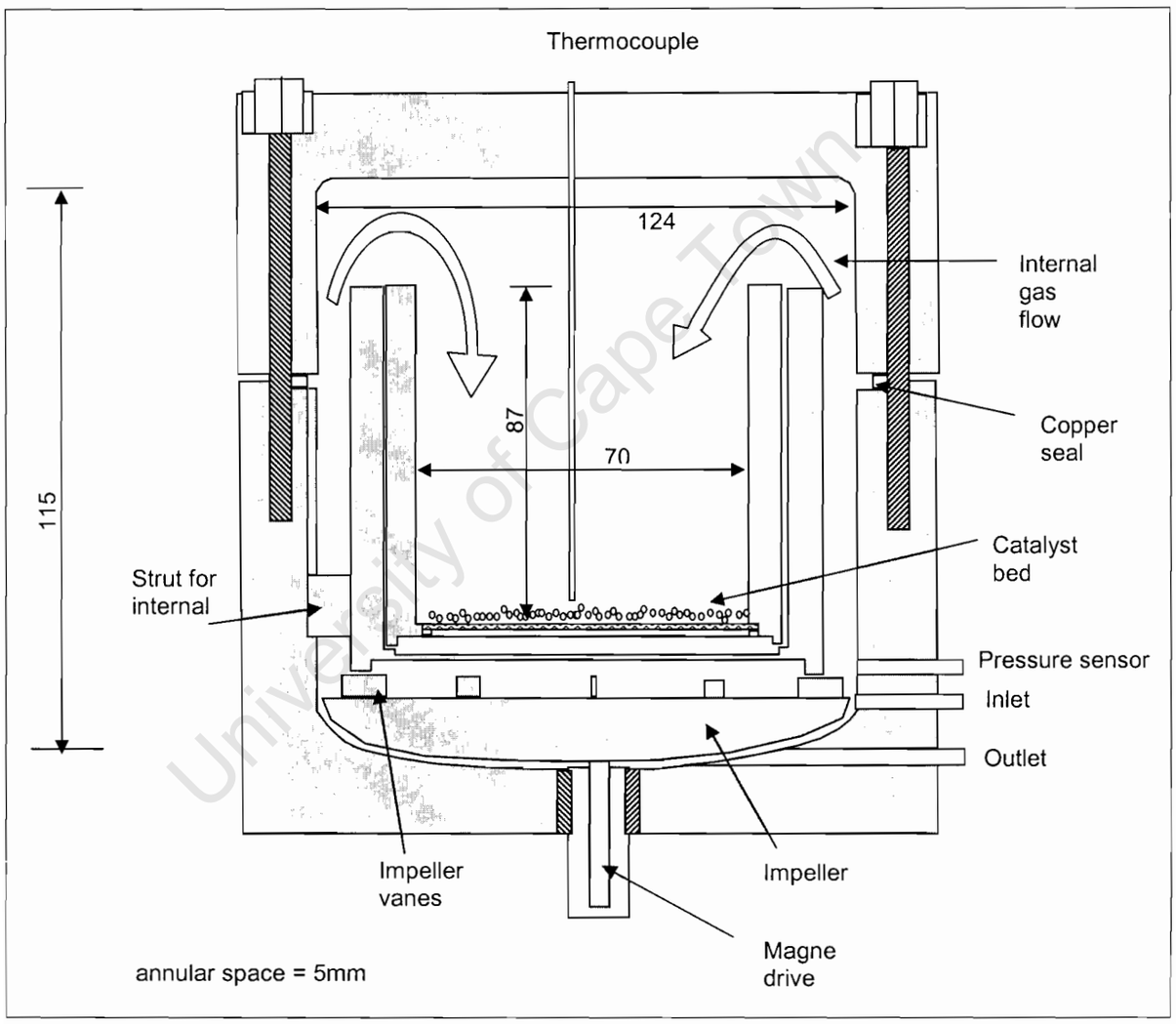


**Figure 2.5**: The Berty micro reactor (dimensions given in millimetre).

### 2.6.2 Sampling

Samples of the feed gas and the hot product gas, before the cold knockout pot, were collected once every 24 hours. Gas samples were collected with evacuated glass ampoules of approximately 2-ml volume. The evacuated ampoule was inserted into a heated sampling device, maintained at 463 K, which allowed for the slow flow of the gaseous hydrocarbon product over the stem of the ampoule. The stem passed through a two pronged fork. By turning the fork the stem of the ampoule was broken and the ampoule was filled with the hot hydrocarbon product from the reactor outlet. The ampoule

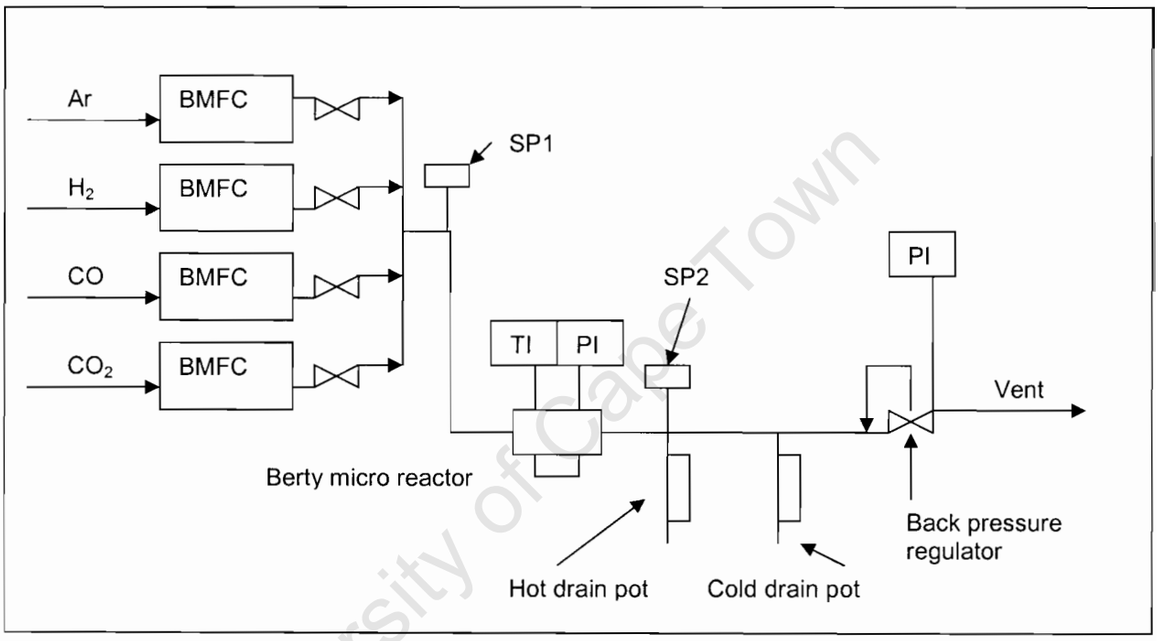


**Figure 2.6:** The reactor outlay with the sample points.

BMFC: Brooks mass flow controller
SP1: Feed gas sampling point
SP2: Hot outlet gas sampling point
TI: Temperature indicator
PI: Pressure indicator

was then sealed with a propane burner and analysed at a later stage. The liquid drainings collected from the cold knockout pot, consisting of water product and an oil product, were collected once every 24 hours and then immediately separated from each other. The temperature of the cold knockout pot was maintained at 283 K.

**Table 2.5**: The operating conditions used for measuring the catalytic activity in the Fischer-Tropsch synthesis.

| **Activation (reduction in pure $H_2$ )** | |
|---|---|
| Temperature, K | 693 |
| Pressure, MPa | 2.0 |
| $pH_2$, MPa | 2.0 |
| Time, hours | 16 |
| Unreduced catalyst mass, g | 5.0 |
| | |
| **Synthesis** | |
| Temperature, K | 603 |
| Pressure, MPa | 2.0 |
| GHSV, $l_N/(g_{cat}.hr)$ | 12.5 |
| P $H_2$, MPa | 1.16 |
| P CO, MPa | 0.28 |
| P $CO_2$, MPa | 0.25 |
| P Ar, MPa | 0.26 |
| P $CH_4$ and inerts, MPa | 0.05 |
| $H_2$/CO at reactor inlet | 4.1 |

### 2.6.3 Analysis of Reactor Samples

The gaseous samples were analysed by gas chromatography, the water product for total carboxylic acid content and oxygenate compounds. The oil samples was analysed for its total carboxylic acid content.

#### 2.6.3.1 Permanent Gases

The reactor feed and outlet gas were analysed for its $H_2$, CO, $CO_2$, Ar and $CH_4$ content. These gases are commonly referred to as the permanent gases.

The analysis was done with a HP gas chromatograph and a Carboxen 1000 column. The sample ampoule was inserted in the sample chamber and the sample chamber and column evacuated to remove any air in the sample loop. The ampoule was broken with a screw type ampoule breaker and the sample distributed itself across the sample loop and the sample was then injected onto the column.

The TCD peak areas of the CO, $CH_4$, $CO_2$ and $H_2$ are then expressed as per the area of the Ar peak on the chromatogram. From the known Ar feed rate into the reactor and a calibrated TCD response the flow rates of the $H_2$, CO, $CO_2$ and $CH_4$ are quantified. From the CO and the $CO_2$ concentration in and out, the percentage CO conversion and percentage CO+$CO_2$ conversions are calculated.

#### 2.6.3.2 Gaseous Hydrocarbon Distribution

For the analysis of the gaseous organic products a HP 6890 gas chromatograph equipped with a flame ionisation detector (FIDGC) was employed. Helium was used as carrier gas. To enable the injection of the ampoule content into the capillary column, a pneumatic ampoule breaker was used. The ampoule was placed in the pneumatic ampoule breaker and the breaker flushed with helium, whilst the ampoule heated up to 423 K. As soon as the pre-column pressure stabilised and the GC oven reached 213 K the ampoule was broken pneumatically. A valve was then switched allowing for the flow of the hydrogen carrier gas into the ampoule breaker. The separation

of the hydrocarbons was achieved with a Petrocol DH 150 (150 m long x 0.25 mm ID coated with a 1 μm methyl silicon stationary phase film) capillary column. The temperature program started off at 213 K, held for 10 minutes, after which it was increased at 10 K per minute to 253 K, and then immediately raised at 2 K per minute to 553 K. The GC was operated in the constant flow mode. The hydrocarbon products are quantified from their response factors and the amount of $CH_4$ as measured from the TCD analysis.

Calculations used in quantifying the gaseous products from the reactor;

$$n_{i,in} = \frac{P_i^c}{P_{Ar}^c} \times \frac{A_{Ar}^{TCD,c}}{A_i^{TCD,c}} \times \frac{A_{i,in}^{TCD}}{A_{Ar,in}^{TCD}} \times n_{Ar}$$

$$n_{i,out} = \frac{P_i^c}{P_{Ar}^c} \times \frac{A_{Ar}^{TCD,c}}{A_i^{TCD,c}} \times \frac{A_{i,out}^{TCD}}{A_{Ar,out}^{TCD}} \times n_{Ar}$$

$$\%\,CO\ conversion = \frac{100 \times (n_{CO,in} - n_{CO,out})}{n_{CO,in}}$$

$$\%\,(CO + CO_2)\ conversion = \frac{100 \times [(n_{CO,in} - n_{CO,out}) - (n_{CO_2,out} - n_{CO_2,in})]}{n_{CO,in} + n_{CO_2,in}}$$

$$n_{fi,in} = \frac{A_{fi}^{FID} \cdot f_{CH_4}^{FID} \cdot M_{CH_4} \cdot n_{CH_4}}{A_{CH_4}^{FID} \cdot f_{fi}^{FID} \cdot M_{fi}}$$

$$n_{fi,out} = \frac{A_{fi}^{FID} \cdot f_{CH_4}^{FID} \cdot M_{CH_4} \cdot n_{CH_4}}{A_{CH_4}^{FID} \cdot f_{fi}^{FID} \cdot M_{fi}}$$

$$S = \frac{\left(n_{fi,out} - n_{fi,in}\right) \times 100 \times C_N}{\left(n_{CO,in} - n_{CO,out}\right) - \left(n_{CO_2,out} - n_{CO_2,in}\right)}$$

Where:

M = catalyst mass in grams.

$A_{i,in}^{TCD}$ = TCD peak area of compound i as a result of the GC analysis on inlet ampoule.

$A_{i,out}^{TCD}$ = TCD peak area of compound i as a result of the GC analysis on outlet gas sample ampoule.

$A_i^{TCD}$ = TCD peak area of compound i

$A_{Ar}^{TCD}$ = TCD peak area of Ar

$A_i^{TCD,c}$ = TCD peak area of compound i in the calibration gas

$A_{Ar}^{TCD,c}$ = TCD peak area of Ar in the calibration gas

$A_{fi}^{FID}$ = peak area of component fi in the FID chromatogram

$A_{CH_4}^{FID}$ = peak area of $CH_4$ in the FID chromatogram.

$C_N$ = Carbon number of hydrocarbon species fi

$f_{CH_4}^{FID}$ = FID correction factor for $CH_4$

$f_{fi}^{FID}$ = FID correction factor for compound fi

$M_{fi}$ = Molar mass of component fi, in g/mole.

$M_{CH_4}$ = Molar mass of $CH_4$ in g/mole.

$n_{Ar}$ = molar flow of argon, mole.$s^{-1}$.

$n_{fi,in}$ = molar flow of hydrocarbon compound fi, in mole.$s^{-1}$.

$n_{fi,out}$ = molar flow of hydrocarbon compound fi, in mole.$s^{-1}$.

$n_{i,in}$ = inlet flow of either $H_2$, CO, $CO_2$ or $CH_4$ in moles.$s^{-1}$

$n_{i,out}$ = outlet flow of either $H_2$, CO, $CO_2$ or $CH_4$ in moles.$s^{-1}$

$P_i^c$ = mole percent of compound i in the reference gas.

$P_{Ar}^c$ = mole percent of Ar in the reference gas.

S = % Carbon atom selectivity, calculated with regards to CO converted to all products, excluding $CO_2$



#### 2.6.3.3 Water Product Analysis

The total quantity of carboxylic acids in the water product was determined with an acid base titration using phenolphthalein as indicator. The quantity of alkali needed to neutralise the acids are determined, and the acidity reported as mg KOH/g of sample used. The oxygenate distribution was determined gas chromatographically with a pona/FID column and detector.

#### 2.6.3.4 Oil Product Analysis

The oil product collected from the reactor was analysed for its total quantity of carboxylic acids. The quantity of alkali (as alcoholic-Alkali) needed to neutralise the acids to the P-Naftolbezene indicator endpoint are determined, and the acidity reported as mg KOH/g of sample used.

# 3 Experimental Results

## 3.1 Chemical Composition

The iron content of the samples was determined using a redox titration, and the concentration of the other elements in the iron catalysts were determined using ICP-AES. The results are reported in Table 3.1

**Table 3.1:** Chemical composition of the catalysts as obtained by wet chemical analysis (the amount of promoter is given as g promoter per 100 g Fe).

| | **Mass % Fe** | **$Na_2O$** | **Cu** | **Cr** | **$Al_2O_3$** |
|---|---|---|---|---|---|
| | | /100 Fe | | | |
| **N** | 67.5 | 0.18 | 0.52 | 0.27 | 0.00 |
| **P(0.2)** | 67.2 | 0.18 | 0.54 | 0.27 | 0.19 |
| **P(0.5)** | 66.9 | 0.18 | 0.51 | 0.30 | 0.46 |
| **P(1.0)** | 66.9 | 0.20 | 0.54 | 0.30 | 0.92 |
| **P(1.5)** | 66.1 | 0.20 | 0.56 | 0.32 | 1.59 |
| | | | | | |
| **B(0.2)** | 66.3 | 0.20 | 0.53 | 0.29 | 0.19 |
| **B(0.5)** | 66.5 | 0.20 | 0.54 | 0.30 | 0.49 |
| **B(1.0)** | 66.1 | 0.22 | 0.57 | 0.32 | 0.96 |



The chemical analysis shows that the elemental composition corresponds reasonably well with the amount of promoter, which was aimed for. The sodium content, recalculated as $Na_2O$, was 0.20±0.014 g $Na_2O$/100 g Fe. The copper content was 0.54±0.02 g Cu/100 g Fe, and the chromium content was 0.30±0.02 g Cr/100 g Fe. The alumina content deviated on average 6% from the intended amount of alumina. The typical deviation showed a lower amount of alumina than intended, with the exception of catalyst P(1.5), which might be attributed to a lower amount of aluminium in the starting aluminium salt,

$Al(NO_3)_3.9H_2O$. A weighing and or analysis error might have contributed to the higher than intended Al content in sample P(1.5).

The oxygen content of the sample was not measured. The difference in mass between the mass analysed and the mass present in the various elements is ascribed to the elements, which were not analysed. The mass balance closes reasonably well if the difference in mass is taken as oxygen.

## 3.2 Physical Characterisation

### 3.2.1 Particle morphology

SEM photos were taken to evaluate the sphericity of the catalyst particles; the sphericity is a mainly a function of the spray drying conditions. The catalyst particles in the SEM images all appear reasonably spherical with small particles also visible. Catalyst P(1.0) shows particles that have indentations.



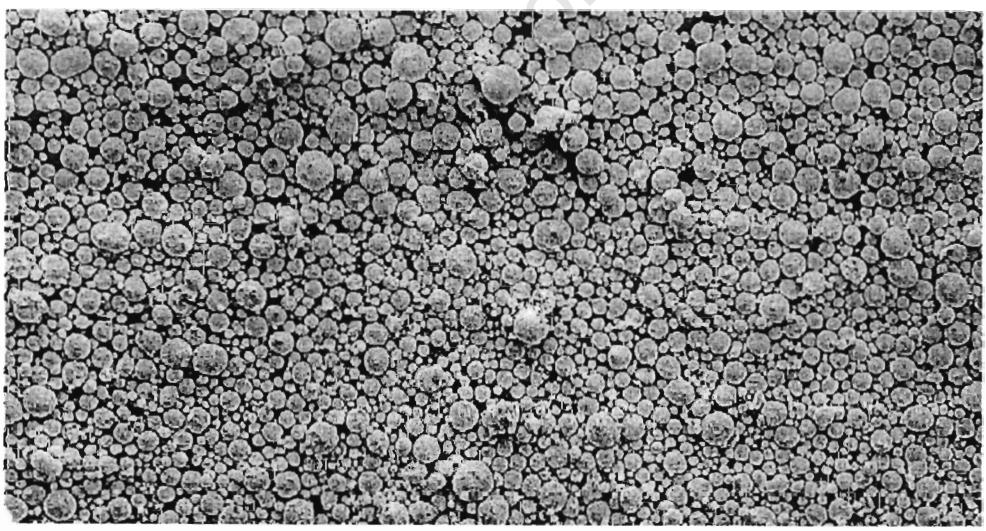

**Figure 3.1a:** SEM image of catalyst N (1cm corresponds to 80 μm).

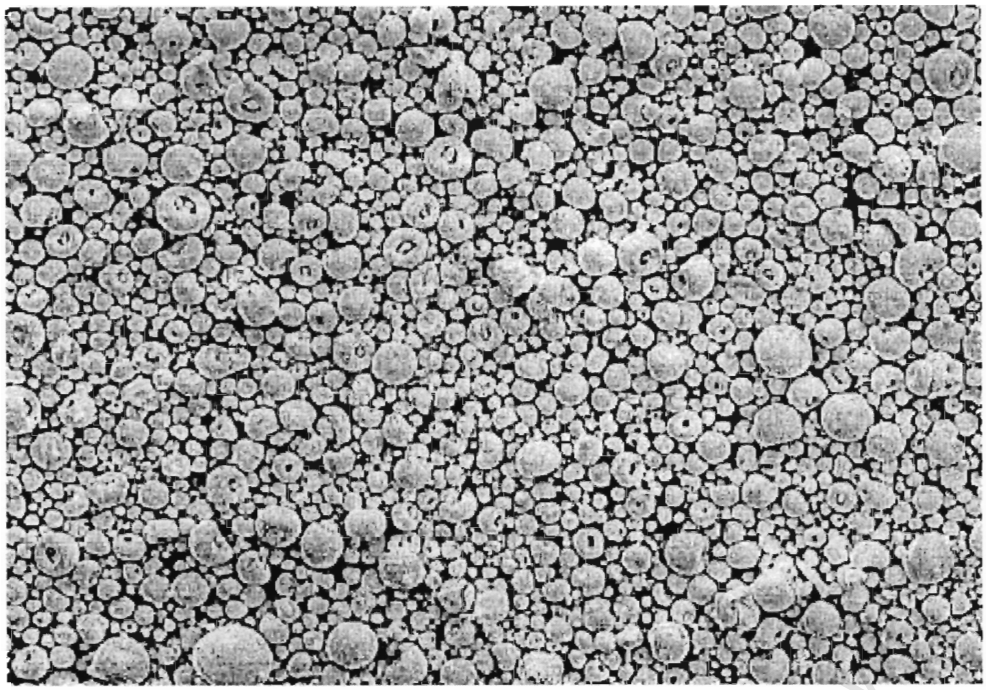

**Figure 3.1b:** SEM image of catalyst P(1.0) (1cm corresponds to 80 μm).

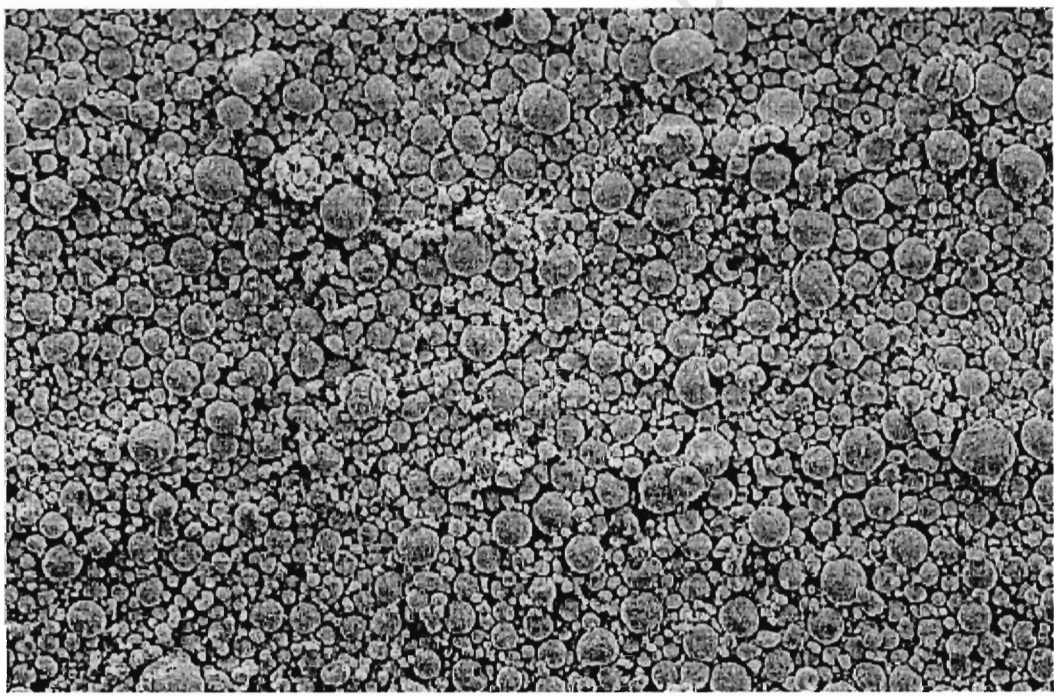

**Figure 3.1c:** SEM image of catalyst B(1.0) (1cm corresponds to 80 μm).

### 3.2.2 Density Measurement Results

The absolute density, particle density and bulk density of the catalysts N, P(1.0) and B(1.0) was investigated (see Table 3.2). According to the results there is no discernable difference between the three catalyst samples in terms of their skeletal, particle and bulk density.

**Table 3.2:** The absolute, particle and bulk density, and pore volume obtained for the catalysts.

| Catalyst Sample | Absolute density by He intrusion | Particle density by MIP | Bulk density by MIP | Pore volume[1] |
|---|---|---|---|---|
| | $g/cm^3$ | $g/cm^3$ | $g/cm^3$ | $cm^3/g$ |
| N | 5.08 | 2.43 | 1.44 | 0.21 |
| P(1.0) | 5.11 | 2.39 | 1.34 | 0.22 |
| B(1.0) | 5.08 | 2.34 | 1.41 | 0.23 |

[1] Pore volume calculated from absolute density and particle density (see equation 3.1)

The absolute density corresponds closely to the density of hematite, $Fe_2O_3$ ($\rho_{Fe2O3}$ = 5.12 $g/cm^3$). This is not surprising since the calcined catalyst particles contained ca. 94-97% $Fe_2O_3$.

The pore volume can be determined using the particle density and the solid density:

$$V_{pore} = \frac{1}{\rho_{particle}} - \frac{1}{\rho_{absolute}} \quad \text{.....(3.1)}$$

The pore volume does not show a great variation, although the pore volume of the calcined catalyst without alumina is slightly less than the ones with alumina. Furthermore, the addition of alumina during the precipitation leads to a slightly lower pore volume than for the catalyst in which the alumina was added prior to spray-drying.

### 3.2.3 Temperature programmed reduction

Figure 3.1 shows the hydrogen consumption in the temperature programmed reduction (TPR) for the catalysts N, P(1.0) and B(1.0). The total amount of hydrogen consumed and the extent of reduction are reported in table 3.3.

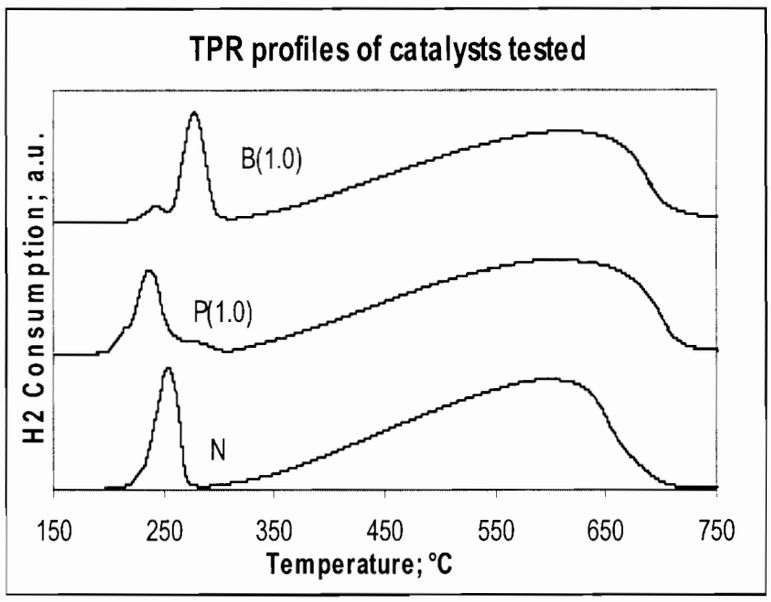


**Figure 3.2:** Temperature programmed reduction profile for catalyst N (bottom) ; P(1.0) (middle) and B(1.0) (top).

Prior to reduction the catalyst samples are essentially hematite, $Fe_2O_3$, albeit promoted with copper, which lowers the reduction temperature (Madon and Taylor, 1981). One mmole of $Fe_2O_3$ will consume three mmoles of $H_2$ to get to the fully reduced phase, see equation 3.2

$$Fe_2O_3 + 3H_2 \leftrightarrow 2Fe + 3H_2O \quad \text{.....(3.2)}$$

According to the stoichiometric equation, 18.8 mmole $H_2$ is needed to fully reduce 1.0 g of $Fe_2O_3$ to the elemental Fe phase. The extent of reduction can then be determined assuming that the catalyst is pure $Fe_2O_3$ prior to reduction.

**Table 3.3:** $H_2$ consumption and the peak temperatures in the temperature programmed reduction of the catalysts.

| | | Catalyst | | |
|---|---|---|---|---|
| | | **N** | **P(1.0)** | **B(1.0)** |
| **First Peak** | | | | |
| Temperature at maximum $H_2$ consumption rate | °C | 254 | 237 | 278 |
| $H_2$ Consumed | mmole/$g_{cat}$ | 1.7 | 1.8 | 1.7 |
| **Second Peak** | | | | |
| Temperature at maximum $H_2$ consumption rate | °C | 598 | 611 | 612 |
| $H_2$ Consumed | mmole/$g_{cat}$ | 11.8 | 12.1 | 11.0 |
| **Total $H_2$ consumed** | mmole/$g_{cat}$ | 13.5 | 13.9 | 12.5 |
| **Extent of reduction** | % | 72 | 74 | 66 |

The TPR curves show roughly two distinct peaks (ca. 250 and 600 °C, respectively). This might be ascribed to a two-stage reduction process. The reduction of hematite might proceed through the formation of magnetite, which is subsequently transformed into metallic iron. It has been reported that wustite, FeO, is thermodynamically metastable with respect to magnetite and iron at temperatures below 843 K. Three reduction peaks are thus not expected (Kock et al., 1985). For a two-stage reduction process proceeding through the formation of magnetite, the first reduction step should account for 11.1% of the total hydrogen consumption. On average the first reduction step accounts for 12.8% of the total hydrogen consumption. This slightly higher than expected value might be ascribed to the reduction of the copper promoter.

For the N catalyst the low temperature reduction peak corresponding to the transformation of hematite to magnetite is sharp and well defined. For catalyst P(1.0) there is a subtle peak on the left shoulder, this is more pronounced in the case of catalyst B(1.0). The peak maximum for catalyst N lies between the

other two catalyst and is slightly higher than catalyst P(1.0). The subtleties in the differences in the low temperature peak must be attributed to the interaction of copper with iron oxide and with alumina, and the interaction of iron oxide with alumina.

The second reduction peak is thought to correspond to the reduction of magnetite to metallic iron. The temperature at which the rate of hydrogen consumption is the highest, is lower for catalyst N than for the alumina promoted catalysts. Alumina is thus inhibiting the rate of reduction of magnetite slightly.

### 3.2.4 Surface Area Analysis.

The BET-surface area ($S_{BET}$) was determined using $N_2$-physisorption at relative pressures of between $0.05 < P/P_0 < 0.2$. To get an indication of the repeatability some of the catalyst samples were analysed in duplicate and the results reported in parentheses in Table 3.4. The pore volume was determined from a single point adsorption total pore volume of pores at a relative pressure, $P/P_0$, of 0.99 (see also table 3.2). This corresponds to pores with a diameter less than 166 nm. The average pore diameter was calculated from the pore volume and the BET surface area assuming cylindrical pores:

$$d_{pore}, \text{in nm} = \frac{4 \times V_{pore}\ (cm^3/g)}{S_{BET}\ (m^2/g)} \times 1000 \quad \ldots(3.3)$$

Figure 3.2 shows the BET surface area as a function of the alumina content (in g/100 g Fe). A significant increase in BET surface area is only observable for the catalyst samples containing more than 0.5g $Al_2O_3$ /100g Fe. Very little variation or trends in the pore volume between the catalyst samples tested were observed. For the catalysts where alumina was added during the co-precipitation (series "P") a decrease in the pore diameter with an increase in the $Al_2O_3$ content is seen. For the catalysts where alumina was added prior to spray-drying (series "B"), there is no discernable trend observed.

**Table 3.4:** The BET surface area, pore volume and average pore size of the catalyst samples (reproducibility measurements in brackets).

| Catalyst sample | $^{a}S_{BET}$ $m^2/g$ | $^{b}V_{Pore}$ $cm^3/g$ | $^{c}d_{pore}$ nm |
|---|---|---|---|
| **N** | 43 | 0.22 | 20 |
| **P(0.2)** | 44 | 0.22 | 20 |
| **P(0.5)** | 42.9 (43.7) | 0.18 (0.18) | 17 |
| **P(1.0)** | 54 | 0.20 | 15 |
| **P(1.5)** | 72.0 (71.8) | 0.19 (0.19) | 11 |
| **B(0.2)** | 46 | 0.21 | 18 |
| **B(0.5)** | 43 | 0.22 | 20 |
| **B(1.0)** | 48.6 (48.8) | 0.23 (0.22) | 19 |

$^{a}S_{BET}$: BET surface area

$^{b}V_{pore}$: Pore volume for pores with a diameter less than 166 nm

$^{c}d_{pore}$: Average pore diameter assuming cylindrical pores (see eq. 3.3)



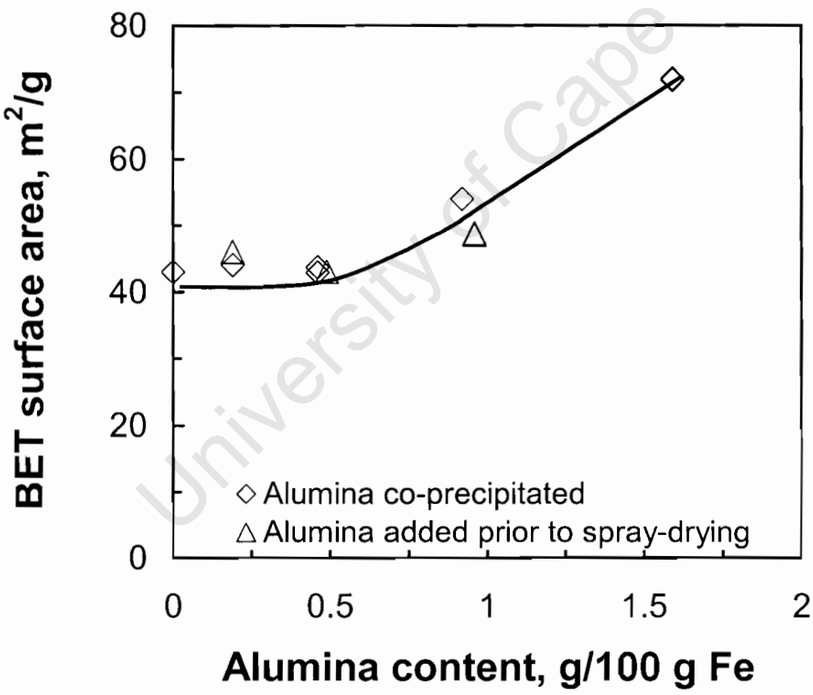


**Graph 3.2:** Variation in the BET surface area with an increase in $Al_2O_3$-content in the catalyst.

According to the IUPAC classification pore sizes of 2 nm to 50 nm are classified as mesoporous. This then classifies these catalysts as mesoporous materials.

### 3.2.5 XRD analysis

Figure 3.3 shows the XRD-patterns of the three catalyst samples N, P(1.0) and B(1.0). The XRD patterns for all three catalysts correspond to the one for hematite. The average crystallite size of $Fe_2O_3$ was determined using the Debye-Scherrrer equation (the measured peak broadening was corrected for the machine line broadening, which was determined from the XRD pattern of NaCl at $2\theta$= 37.1° and 53.4° to be 0.21°). The diffraction peak at 38.6° was used to determine the average crystallite size:

N: 121 Å

P(1.0): 125 Å

B(1.0): 140 Å

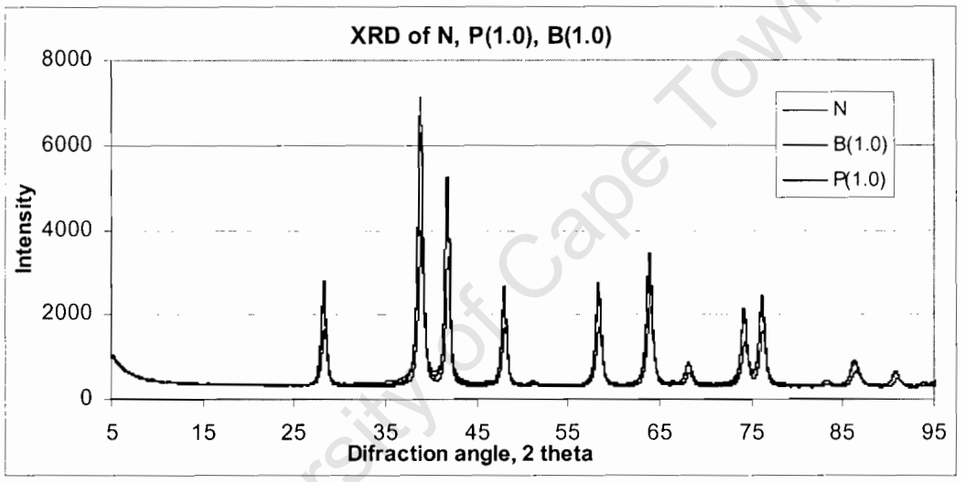


**Figure 3.3:** XRD-patterns of the catalysts N, P(1.0) and B(1.0) catalysts.



### 3.2.6 Particle Size Distribution

The spray drying conditions, such as variations in the feed rate, the slurry viscosity, and temperature fluctuations are expected to have a large influence on the particle size of the final catalyst. Table 3.5 shows the cumulative particle size distribution of the spray-dried catalyst samples (see also Figure 3.4). The mean particle size was almost constant, which indicates no

significant difference in the operating conditions during the spray drying action.

**Table 3.5:** Cumulative particle size distribution of the prepared, spray-dried and calcined samples.

| | N | P(0.5) | B(0.5) | P(1.0) | B(1.0) | P(1.5) |
|---|---|---|---|---|---|---|
| µm | | | | | | |
| 150 | 100 | 100 | 100 | 100 | 100 | 100 |
| 124 | 98 | 98 | 95 | 99 | 96 | 97 |
| 92.1 | 93 | 92 | 89 | 93 | 89 | 88 |
| 83.4 | 91 | 88 | 85 | 89 | 85 | 84 |
| 75.6 | 87 | 82 | 80 | 85 | 80 | 78 |
| 62.1 | 73 | 65 | 63 | 72 | 63 | 65 |
| 46.2 | 40 | 34 | 35 | 44 | 35 | 43 |
| 34.3 | 20 | 16 | 20 | 24 | 20 | 24 |
| 21.0 | 6 | 4 | 7 | 8 | 7 | 7 |
| 15.6 | 3 | 2 | 4 | 4 | 4 | 3 |
| 11.6 | 2 | 1 | 2 | 2 | 2 | 2 |
| 7.8 | 1 | 0 | 1 | 1 | 1 | 1 |
| | | | | | | |
| Mean, µm | 51 | 54 | 55 | 51 | 55 | 51 |



### 3.3 Attrition Resistance of the Catalysts

The resistance towards impact attrition was measured by the jet-impingement test and quantified by the breakage index (see equation 2.5). Prior to this test the catalyst samples were sieved to 38-63 µm. Figure 3.5 shows that the particle size distribution of all selected samples are similar after being sieved. The mean particle size of the samples, before jet impingement, also reflects a constant particle size distribution (see Table 3.6).

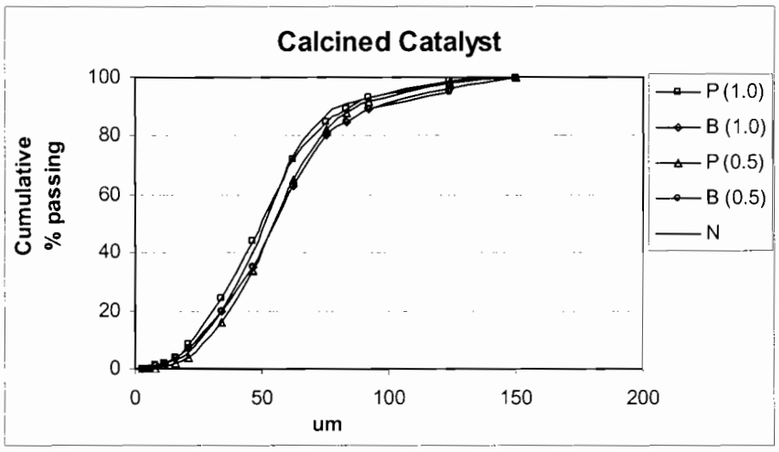


**Figure 3.4:** Cumulative particle size distribution of the prepared, spray-dried and calcined samples.

The particle size distribution was expected to be similar before jet impingement, since the samples were sieved to 38-63 µm. This constant particle size distribution makes the interpretation of the breakage index (BI) results easier. The breaking index is a measure for the relative shift (in %) in the mean particle size. A comparison of the particle size distribution before and after jet impingement is shown in Figures 3.6-9.



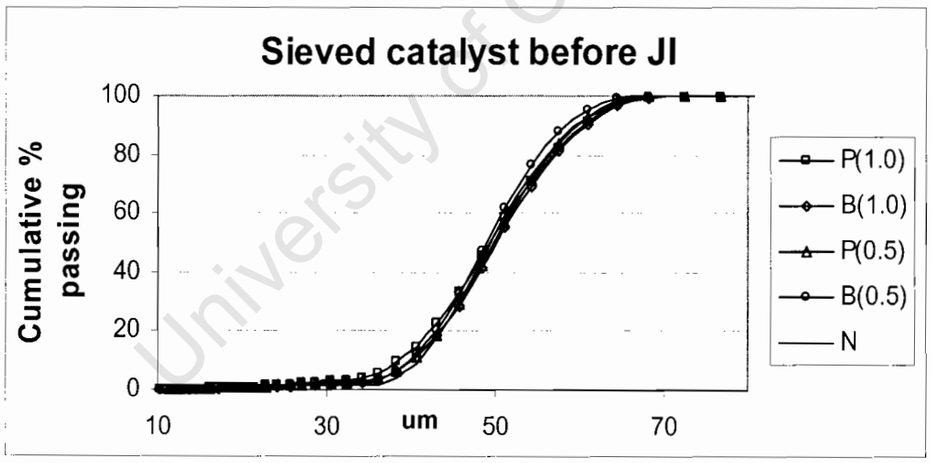


**Figure 3.5:** Cumulative particle size distribution of the samples prior to jet impingement, JI (samples were sieved to 38-63 µm).

**Table 3.6:** Cumulative particle size distribution, mean particle size before jet impingement (BJI) and after jet impingement (AJI) of selected sieved samples and breaking index (BI).

| | N | | P(0.5) | | B(0.5) | | P(1.0) | | B(1.0) | |
|---|---|---|---|---|---|---|---|---|---|---|
| µm | BJI | AJI | BJI | AJI | BJI | AJI | BJI | AJI | BJI | AJI |
| | | | | | | | | | | |
| 72.4 | 100 | 100 | 100 | 100 | 100 | 100 | 100 | 100 | 100 | 100 |
| 60.9 | 93.0 | 94.0 | 92.9 | 96.2 | 95.3 | 91.0 | 90.7 | 95.2 | 90.4 | 93.5 |
| 57.5 | 84.8 | 86.9 | 83.7 | 92.0 | 87.7 | 83.0 | 82.0 | 90.7 | 81.0 | 86.8 |
| 54.3 | 73.1 | 77.0 | 71.1 | 86.0 | 76.2 | 73.0 | 70.9 | 84.6 | 68.8 | 78.0 |
| 51.3 | 59.1 | 65.0 | 56.7 | 78.6 | 62.0 | 61.9 | 58.3 | 77.4 | 55.0 | 67.6 |
| 48.4 | 44.0 | 52.3 | 42.1 | 70.3 | 46.9 | 50.8 | 45.3 | 69.5 | 41.2 | 56.8 |
| 45.7 | 29.8 | 40.1 | 29.1 | 61.8 | 32.6 | 40.8 | 33.3 | 61.4 | 28.8 | 46.6 |
| 43.1 | 17.8 | 29.7 | 18.5 | 53.8 | 20.7 | 32.6 | 23.0 | 53.8 | 18.6 | 37.7 |
| 38.4 | 4.1 | 16.2 | 6.3 | 40.7 | 6.3 | 22.3 | 9.4 | 41.2 | 6.4 | 25.5 |
| 32.3 | 1.4 | 10.7 | 2.6 | 35.9 | 2.2 | 16.9 | 3.4 | 29.0 | 2.0 | 18.2 |
| 22.9 | 0.8 | 6.8 | 1.0 | 15.1 | 1.0 | 10.7 | 1.4 | 14.2 | 0.8 | 10.9 |
| 16.2 | 0.3 | 4.4 | 0.3 | 7.6 | 0.3 | 7.1 | 0.5 | 6.5 | 0.2 | 6.9 |
| 12.9 | 0.2 | 3.2 | | 4.9 | 0.1 | 5.2 | 0.3 | 3.9 | | 4.9 |
| 8.6 | | 1.9 | | 2.3 | | 3.1 | | 1.7 | | 2.9 |
| 6.8 | | 1.5 | | 1.8 | | 2.4 | | 1.3 | | 2.2 |
| | | | | | | | | | | |
| Mean, µm | 49.7 | 46.0 | 49.7 | 39.5 | 48.8 | 45.1 | 49.2 | 39.9 | 50.2 | 43.7 |
| BI | 7.4 | | 20.5 | | 7.6 | | 18.9 | | 12.8 | |



The breaking index for the catalyst sample without alumina (sample "N") is rather small (7.4), and the catalyst undergoes very little abrasion. Particle break-up cannot be observed with these particles. After jet impingement some particles in the range of 20-30 µm are formed, but the particles are still mainly between 38-63 µm.

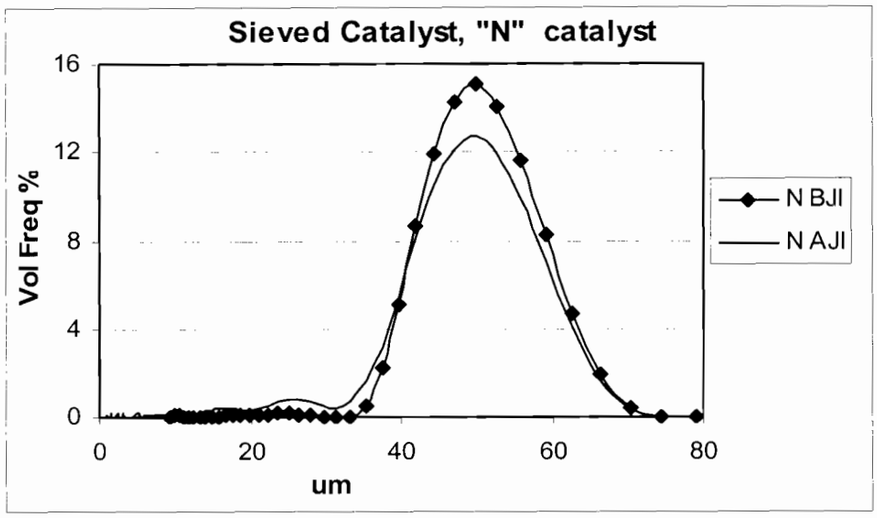


**Figure 3.6:** Particle size distribution of the sieved catalyst without alumina (sample N) before jet impingement (BJI) and after the jet impingement action (AJI).

The samples, where alumina was co-precipitated, (sample P) show a high breaking index (ca. 19), which is hardly affected by the alumina content. Figure 3.7 shows the particle size distribution for these samples. There is an increase in the amount of fine material observed after the jet impingement. This might be ascribed to both break-up and abrasion occurring.



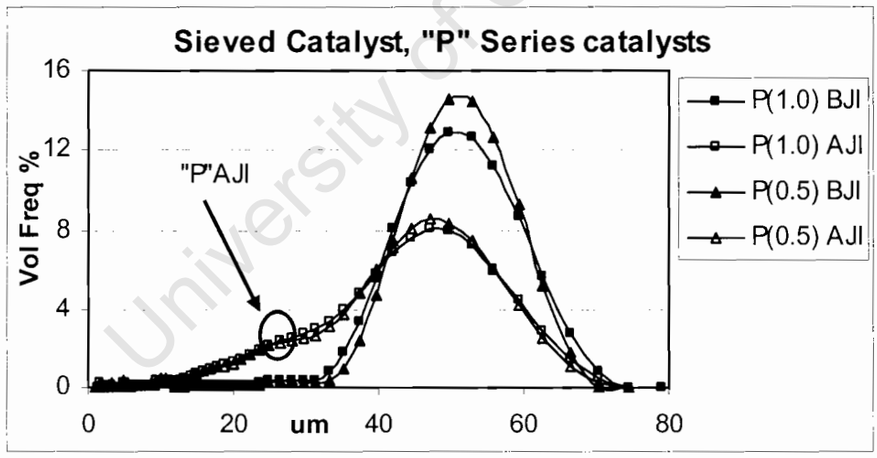


**Figure 3.7:** Particle size distribution of the sieved catalyst with co-precipitated alumina (samples "P") before jet impingement (BJI) and after the jet impingement action (AJI).

Figure 3.8 shows the volume frequency percent particle size distribution for the catalysts where alumina was added prior to spray-drying ("B" series). The mean has decreased by 4μm and 7 μm for the B(0.5) and B(1.0) catalysts. There is less abrasion observed compared to the catalysts in which alumina was co-precipitated ("P" series sample).

The breakage index as a function of the alumina content in the various samples is shown in Figure 3.9. From Table 3.6 and Figure 3.10 it is clear that the samples prepared with the $Al_2O_3$ added after the precipitation step prior to spray-drying ("B" samples) has lower breaking index than the samples with alumina co-precipitated ("P" samples). The sample with no alumina added has the lowest breaking index of all the samples tested and thus has the highest resistance towards impact attrition as measured by the jet impingement test.

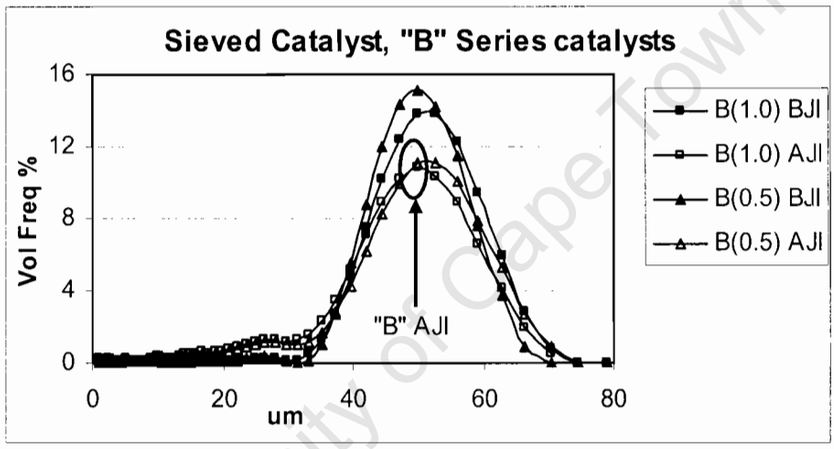


**Figure 3.8:** Particle size distribution of the sieved catalyst with alumina added prior to spray-drying (samples "B") before jet impingement (BJI) and after the jet impingement action (AJI).

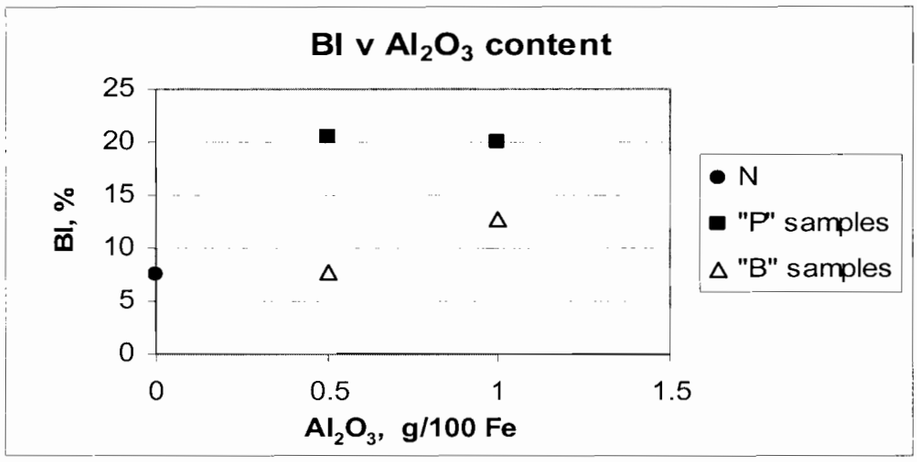


**Graph 3.10:** The breakage index as a function of the $Al_2O_3$ content of the samples.

## 3.4 PERFORMANCE IN THE FISCHER-TROPSCH SYNTHESIS

The Fischer-Tropsch synthesis performance of three of the prepared catalyst samples was tested in a micro-reactor. Table 3.7 summarises the reaction conditions and the activity and selectivity obtained. The results are the average synthesis performance reported during the time period of 72-120 hours on line. The reactor partial pressures are different from those reported for the feed in section 2.6.1 due to the high internal recycle in the Berty micro reactor.

Due to the high conversion of CO in the reactor the partial pressure of CO in the reactor is very low compared to that of the $H_2$. The $H_2$/CO ratio inside the reactor is then approximately five times higher that that of the feed gas ratio.

The partial pressure for the $CO_2$ as a product of the WGS reaction in the reactor is also higher than that in the feed gas. The water-gas shift reaction is not quite at equilibrium yet, since the ratio of the partial pressure of hydrogen and carbon dioxide relative to the partial pressures of carbon monoxide and water should be 27.3 (calculated from HSC version 4.0 software). This indicates that for the P(1.0) and B(1.0) catalyst there is more water than at equilibrium.

**Table 3.7:** Average conditions between 72 and 120 hrs on-line in the Fischer-Tropsch synthesis.

| | N | P(1.0) | B(1.0) |
|---|---|---|---|
| **Reactor partial pressures** | | | |
| $pH_2$, MPa | 0.87 | 0.82 | 0.84 |
| pCO, MPa | 0.041 | 0.045 | 0.044 |
| $pH_2O$, MPa | 0.27 | 0.27 | 0.27 |
| $pCO_2$, MPa | 0.32 | 0.32 | 0.32 |
| Reactor $H_2$/CO | 21.5 | 18.5 | 19.6 |
| $\left(p_{CO_2} \cdot p_{H_2} / p_{CO} \cdot p_{H_2O}\right)_{reactor}$ | 26.5 | 21.9 | 23.1 |
| **Synthesis performance** | | | |
| CO conversion, % | 88 | 87 | 87 |
| $CO+CO_2$ conversion, % | 44 | 44 | 44 |
| $r_{FT}$, (µmol CO converted to FT products)/($g_{cat}$.s) | 25 | 25 | 25 |
| $r_{WGS}$, (µmol $CO_2$ produced)/($g_{cat}$.s) | 1.9 | 1.4 | 1.4 |
| **Selectivity, C-%** | | | |
| $CH_4$ | 12 | 16 | 14 |
| $C_2^{tot}$ | 11 | 12 | 11 |
| $C_3^{tot}$ | 16 | 16 | 15 |
| **Molar ratio alkene to alkane** | | | |
| $C_2$ | 2.5 | 1.8 | 2.6 |
| $C_3$ | 9.0 | 7.8 | 9.5 |
| **Chain growth probability (total HC distribution)** | 0.66 | 0.66 | 0.68 |



The CO and $CO+CO_2$ conversion as a function of time on-line are given in Figures 3.10 and 3.11. The $CO+CO_2$ conversion gives an indication of the amount of hydrocarbon product formed. The activity, measured as the percentage CO converted, of the three catalysts tested did not differ significantly. The same can be said for the $CO+CO_2$ conversion.

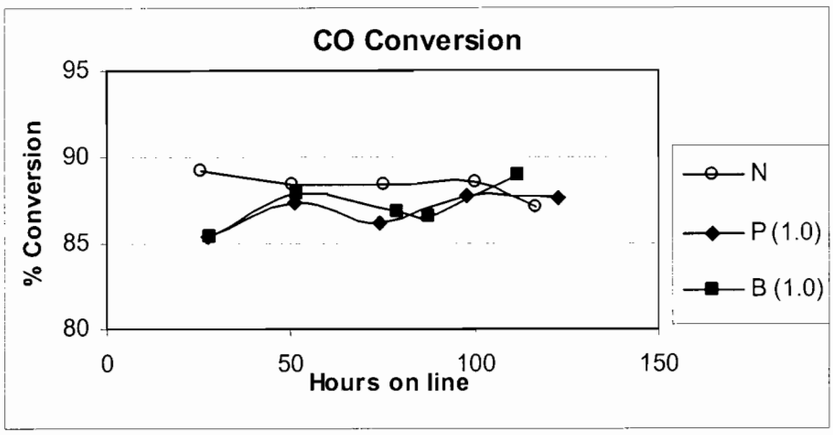


**Figure 3.10:** CO conversion as a function of the time on-line.

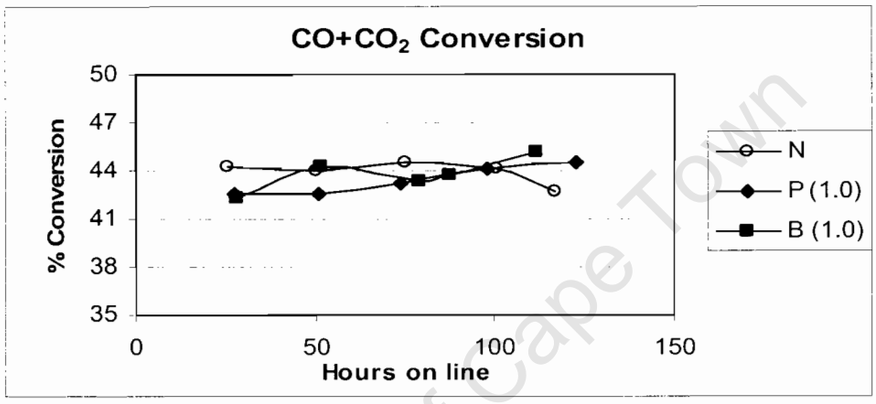


**Figure 3.11:** Conversion of $CO+CO_2$ (as an indicator for the conversion yielding hydrocarbons) as a function of time on-line.

The hydrocarbon products are formed through a surface polymerisation. Figure 3.12 shows the selectivity for the formation of hydrocarbons in carbon-% as a function of carbon number as an average between 72 and 120 hrs on-line. The methane selectivity is higher with the catalysts containing alumina. The catalyst, where alumina was co-precipitated, showed the highest methane selectivity. The selectivity for the formation of $C_3$-hydrocarbons is the highest, which could have been expected based on the experimental conditions of the high temperature Fischer-Tropsch synthesis (see figure 1.10 for a theoretical product distribution).

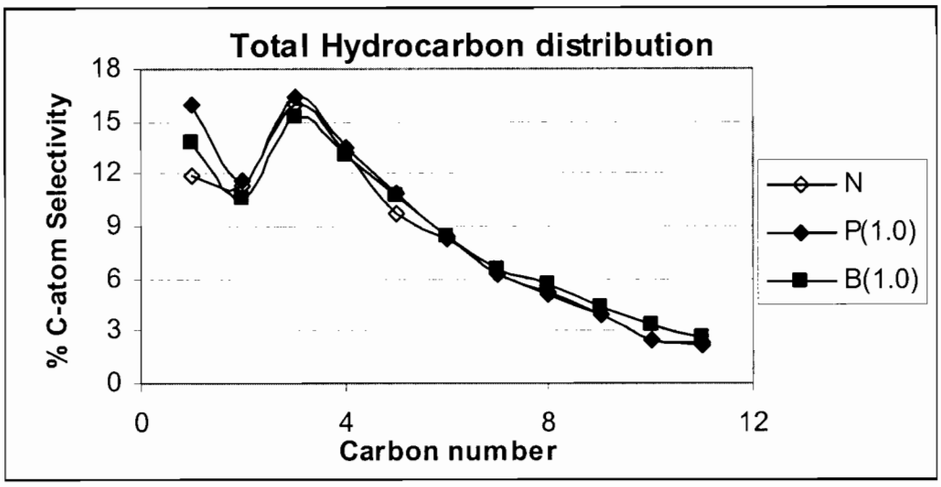


**Figure 3.12**: Hydrocarbon distribution in carbon-% as obtained on the three catalysts tested.

The average Anderson-Schulz-Flory distribution (averaged for time on-line between 72 and 120 hrs) for the total hydrocarbons is shown in Figure 3.13. The alpha plot of the hydrocarbon distribution is expected to follow an Anderson Shultz Flory product distribution. The hydrocarbon distribution and the corresponding alpha plots are given in Graphs 3.13 to 3.15. The slope of the straight line corresponds to the chain growth probability. The plot is reasonably linear between $C_3$ and $C_{11}$. A chain growth probability of 0.66 – 0.68 was determined (see Table 3.7). The methane selectivity is slightly higher and the selectivity for the $C_2$ hydrocarbons is slightly lower than what would be obtained by extrapolating from $C_3$ to $C_{11}$. The calculation did not include the selectivity for the oxygenated compounds.

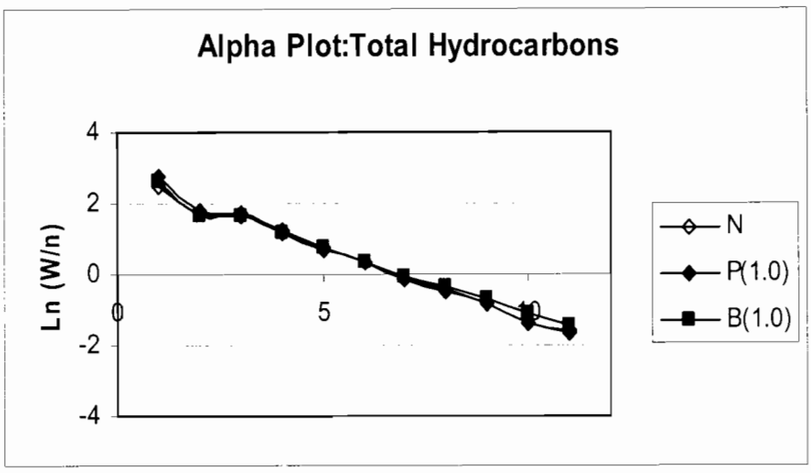


**Figure 3.13:** Anderson-Schulz-Flory plot for the total hydrocarbon distribution.

The Anderson-Schulz-Flory plot for the 1-alkenes (see Figure 3.13) is linear from carbon number 3 onwards. The value for ethene is lower than what the trend predicts, this is normally explained in terms of ethene re-adsorption (Iglesia et al., 1991)

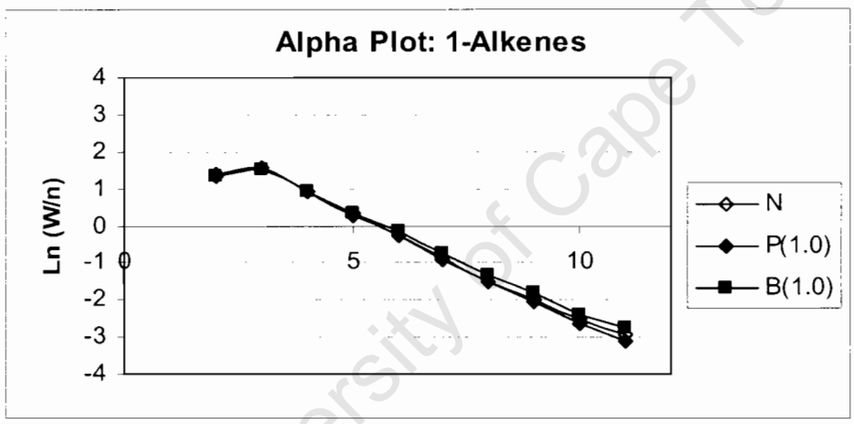


**Figure 3.14:** Anderson-Schulz-Flory plot for the 1-alkene distribution.

The Anderson-Schulz-Flory plot of the n-alkanes (see Figure 3.15) shows that both methane and ethane values are higher than what was expected from extrapolation of the longer chain n-alkanes. Ethene re-adsorption and subsequent hydrogenation will lead to ethane formation and might explain the positive deviation here.

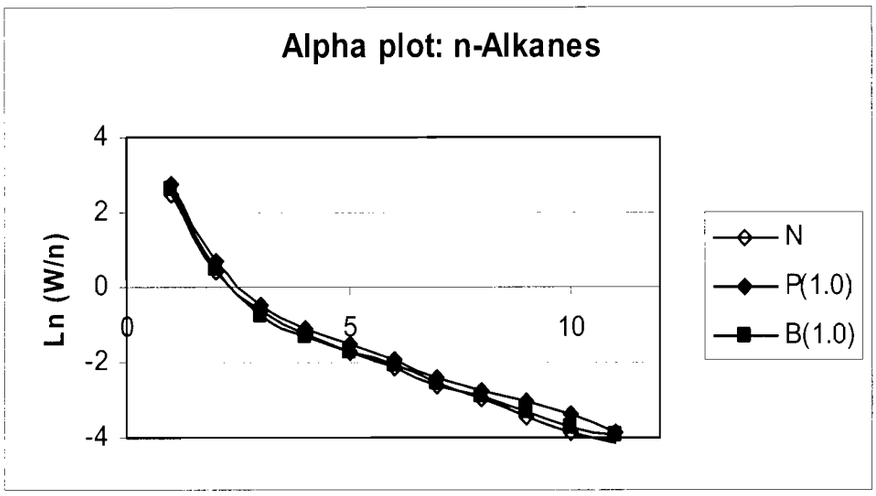


**Figure 3.15:** Anderson-Schulz-Flory plot for the n-alkane distribution.

The molar ratio of ethene to ethane as a function of time on-line is given in Figure 3.16. The molar ratio of ethene to ethane ratio is significantly lower for the catalyst in which alumina was co-precipitated compared to the other two catalysts. The molar ratio of propene to propane is also lower for the catalyst in which alumina is co-precipitated (see Table 3.7). This might indicate that the catalyst with co-precipitated alumina is better able to hydrogenate primarily formed olefins in a secondary hydrogenation reaction.

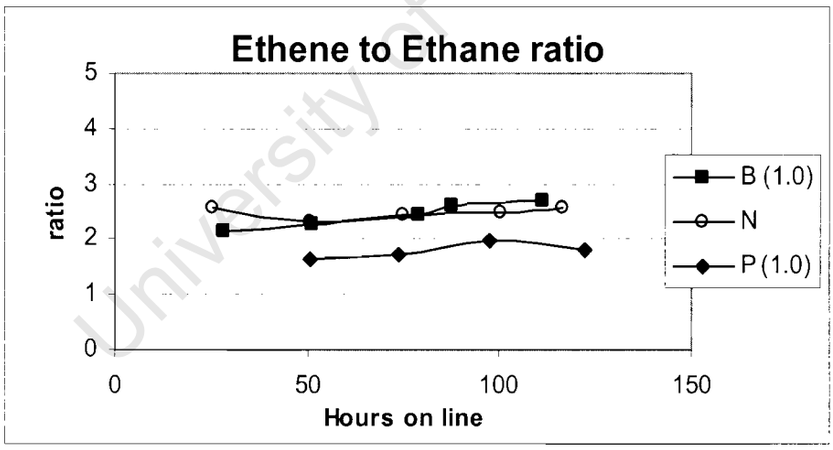


**Figure 3.16:** Molar ratio of ethene to ethane as a function of time on-line.

Table 3.8 shows the oxygenates found in the water product drained from the reactor. The acid number obtained on both the water product and oil product is also given. The catalyst without alumina (series “N”) had the highest alcohol production and the highest acid number. The catalyst in which alumina was co-precipitated made more ketones.

**Table 3.8:** Oxygenate and acid number analysis of the liquid phase drained from the reactor.

| | **N** | **P(1.0)** | **B(1.0)** |
|---|---|---|---|
| | % (m/m) | % (m/m) | % (m/m) |
| Acetaldehyde | 0.102 | 0.094 | 0.056 |
| MEK | 0.097 | 0.146 | 0.092 |
| Acetone | 0.39 | 0.53 | 0.36 |
| Methanol | 0.081 | 0.086 | 0.059 |
| Iso-Propanol | 0.20 | 0.24 | 0.20 |
| N-Propanol | 0.492 | 0.345 | 0.297 |
| N-Butanol | 0.203 | 0.145 | 0.171 |
| Ethanol | 2.52 | 1.61 | 1.43 |
| TOTAL NAC’s | 4.52 | 3.57 | 2.96 |
| Acid number, mg KOH/g | | | |
| Water | 4.7 | 3.7 | 3.4 |
| Oil | 3.9 | 2.5 | 2.6 |

# 4 Discussion

In the study presented here, a small amount of binder, $Al_2O_3$, was added to the catalyst formulation. The maximum amount of $Al_2O_3$ added to the spray-dried catalyst was 1.6 g $Al_2O_3$ per 100 g of iron. Aluminium nitrate was either added during the precipitation step or just prior to the spray-drying step in the catalyst preparation. The role of a binder in the catalyst was expected to increase its attrition resistance, while the low alumina content was expected to exert only a marginal effect on the catalyst performance.

## 4.1 Effect of binder on the physical characteristics of the catalysts

The resistance of the calcined catalyst samples towards attrition was measured by impact attrition. It has been shown in literature (Sudsakorn et al., 2001; Zhao et al., 2001) that there is a decrease in the resistance towards attrition upon an increase in the structural promoter ($SiO_2$) content of precipitated iron catalysts. It has also been shown (Sudsakorn et al. 2001) that the point of addition plays a role in the attrition resistance.

Table 4.1 summarises the characteristics of the particle size distributions obtained. In this study the attrition resistance was measured by the breaking index. The particle size distributions of all freshly calcined spray-dried catalyst particles before jet impingement measurement (BJI) are very similar with an average particle size of ca. 49 μm, a standard deviation of 8 μm and a skewness of –2.3 μm, despite the fact that the SEM images showed a relatively large number of small particles. These particles were sieved out prior to the impact attrition test.

The generally small decrease in the mean particle size upon the attrition testing indicates that the main mechanism of attrition is abrasion with possibly some break-up occurring for the “P” series catalysts.

**Table 4.1:** Average particle size ($\bar{d}_p$), standard deviation, σ, skewness, s, of the obtained particle size distributions and the breaking index.

| | $\bar{d}_p$, μm[1] | σ, μm[2] | s, μm[3] | **Breaking index, BI** |
|---|---|---|---|---|
| N (BJI) | 49.7 | 7.7 | -2.2 | 7.4 |
| N (AJI) | 46.0 | 12.3 | -3.9 | |
| P 0.5 (BJI) | 49.7 | 8.2 | -2.6 | 20.5 |
| P 0.5 (AJI) | 39.5 | 14.3 | -3.0 | |
| P 1.0 (BJI) | 49.2 | 9.2 | -2.5 | 18.9 |
| P 1.0 (AJI) | 39.9 | 14.2 | -2.7 | |
| B 0.5 (BJI) | 48.9 | 7.7 | -2.5 | 7.6 |
| B 0.5 (AJI) | 45.1 | 14.7 | -3.9 | |
| B 1.0 (BJI) | 50.2 | 8.4 | -2.2 | 12.8 |
| B 1.0 (AJI) | 43.7 | 14.2 | -3.7 | |

$$^1\bar{d}_p = \int_0^\infty d_p \cdot F \cdot dd_p \; ; \; ^2\sigma^2 = \int_0^\infty (d_p - \bar{d}_p)^2 \cdot F \cdot dd_p \; ; \; ^3s^3 = \frac{1}{\sigma^{1.5}} \int_0^\infty (d_p - \bar{d}_p)^3 \cdot F \cdot dd_p$$

(With F the frequency distribution of the particle size distribution)

The method of addition of alumina to the catalyst affects the attrition resistance significantly. The co-precipitation of alumina seems to lower the attrition resistance of the catalyst (P-series of catalyst), whereas the addition of aluminium nitrate to the re-slurried catalyst precursor prior to spray-drying does not seem to affect the attrition resistance of the obtained catalysts too negatively. The catalyst precursors obtained after spray-drying, in which aluminium was co-precipitated ("P"-series), were spherical, but a number of the catalyst particles had indentations. The role that these indentations played in the observed attrition resistance of the "P" series catalyst samples is not clear, but it can be reasonably well expected that these particles will have a lower resistance towards impact attrition.

Increasing the alumina content had no effect on the attrition resistance when added during the co-precipitation step. However, increasing the alumina content did adversely affect the attrition resistance, if aluminium nitrate was added to the re-slurried catalyst prior to spray-drying ("B"-series).

It has been previously reported that the BET surface area increases with an increase in alumina or silica promoter added as a structural promoter (Zhao et al., 2001; Dry, 1981). It must however be noted that in general structural promoters are added in much higher concentrations that what was done in this study. In this study the BET-surface area increases with increasing alumina content, if alumina is co-precipitated. The increase in the BET surface area becomes only apparent at higher alumina loading (larger than 0.5 g/100 g Fe). This is ascribed to the low levels of $Al_2O_3$ added in the case of the 0.2 $Al_2O_3$/100Fe. The increase in the BET-surface area is not apparent for the case when aluminium nitrate is added prior to spray-drying to the re-slurried catalyst.

The particle, absolute and bulk densities do not show a significant variation between the three catalysts tested. This is ascribed to the low concentrations of alumina added to the catalysts tested. In literature it has been reported that the particle density is directly related to the attrition resistance of precipitated iron catalysts (Zhao et al., 2001; Sudsakorn et al., 2001). This does not seem to be the case in this study.

The pore volume, as determined from the BET surface area analysis at a P/Po value of 0.99, of the "P" series catalysts did not vary with an increase in the alumina concentration whilst those of the "B" series catalysts appear to be slightly higher than that of the "P" series catalyst. Because of the slightly different BET surface area results the calculation for the average pore diameter shows that for the P series catalysts there is a decrease in the adsorption average pore diameter. This then means that the number of pores must have increased to cause an increase in the $S_{BET}$. For the B series catalyst there is not a discernable

difference between the pore diameter and the alumina loading in the catalysts. This then leads to the conclusion that the number of pores must have decreased.

The attrition tests performed in this study can only attest to the resistance of the calcined catalyst particles against physical attrition. Chemical attrition is expected to strain the catalyst particles stronger during catalyst reduction and the Fischer-Tropsch synthesis. It is therefore recommended that the jet-impingement test apparatus is modified to handle reduced iron catalyst particles.

## 4.2 Effect of binder on the reduction behaviour

The reduction behaviour of the catalyst was tested using temperature programmed reduction (TPR). The three catalysts tested show comparable $H_2$ consumption per peak observed. According to the amount of $H_2$ consumed for the first peak it would seem as if the there was complete reduction of the hematite to magnetite (theoretical amount needed only 11.1 % of total $H_2$ consumed). The conversion of magnetite to elemental iron did not proceed to completion for any of the three catalysts tested.

The results indicate that the reduction of hematite to magnetite for the catalyst P(1.0) was easier than for the other two catalysts tested. The B(1.0) catalyst had the highest temperature for the transformation. This seems to indicate that the P(1.0) had a higher hydrogenation ability that either of the catalysts tested. This might indicate some hydrogen transfer ability of finely dispersed alumina in the sample.

In the B(1.0) catalyst there is a small peak on the left shoulder, at 247 °C, of the first reduction peak. There is also a small poorly defined peak at the right shoulder, at 282°C, of the first reduction peak of the P(1.0) catalyst. The first reduction peak of the "N" catalyst is a sharp peak with a maximum rate of reduction at 257°C. The appearances of the small peaks on the shoulder of the

P(1.0) and B(1.0) catalysts suggests that there are some iron-alumina species present in the P(1.0) and B(1.0) catalyst respectively.

The second large reduction peak shows that there is not a big difference in the final reduction step, the conversion of $Fe_3O_4$ to elemental Fe for all the tested catalysts.

### 4.3 Effect of binder on the catalytic activity and selectivity

The activity of three different catalysts in the Fischer-Tropsch synthesis was investigated, viz. N, P(1.0) and B(1.0). The comparison of the performance of these catalysts will allow some insight in whether the low amount of binder added in this study will affect the performance in the Fischer-Tropsch synthesis. This is a priori not expected, since the alumina content is very low, the BET-surface area in the calcined catalysts are approximately identical (which is further substantiated by an approximately constant crystal size of hematite in the catalyst precursor) and the expected degree of reduction is similar (based on the TPR-profile).

The synthesis results show essentially no difference in the Fischer-Tropsch activity between the three catalysts evaluated in the period between 72 and 105 hours on-line, although there appears to be scatter in the data.

The water-gas shift activity has decreased upon addition of alumina to the catalyst formulation. There is no difference between the P(1.0) and B(1.0) catalysts. Bukur et al. (1990) also observed a decrease in the water gas shift activity upon addition of silica as a binder to a co-precipitated iron catalyst.

The chain growth probability for the total hydrocarbons, the 1-alkenes and the n-alkanes are all identical for the three catalyst tested. This might be attributed to the low levels of aluminium added to two of the catalysts.

The molar content of ethane in the fraction of organic product compounds is higher than expected (see Figure 3.15). This is ascribed to ethene re-adsorption and subsequent hydrogenation (Iglesia et al., 1991). Conversely the molar content of ethene in the fraction of organic product compounds is lower than expected.

The ethene to ethane ratio for the P(1.0) catalyst is less than those of the other two catalysts tested and the $CH_4$ content is higher. This indicates that the catalyst in which the aluminium was co-precipitated has a stronger hydrogenation ability than the catalyst in which the aluminium was added to the slurry before spray drying.

The TPR profile of the P(1.0) catalyst also showed a lower onset temperature for the hematite to magnetite reduction step. This observation can also be explained in terms of the P(1.0) catalysts having a higher hydrogenation ability.

Bukur et al. (1990a and 1990b) commented on conflicting results reported in previous literature on the influence of promoters and binder/support effects on oxygenate selectivities. They did report a gradual decrease in the selectivity towards oxygenates upon an increase in the alumina content of the catalysts. In this study a decrease in the amount of oxygenates (non acid chemicals and the acid content) in the water product from the reactor was also found. The reason why more acetone and methyl-ethyl-ketone was produced by the P(1.0) catalyst is uncertain.

# 5 Conclusion

Two series of precipitated iron catalysts containing alumina as a possible attrition resistance enhancement promoter were prepared. In the one series aluminium nitrate was added during the precipitation step; in the other the aluminium nitrate was added to a re-slurried filter cake just prior to spray drying. The nominal composition was $0.2Na_2O/0.5Cu/0.3Cr/xAl_2O_3/100$ Fe, with x = 0.2, 0.5, 1.0, 1.5. The base case catalyst contained all the promoters with the exception of alumina.

The addition of the aluminium in the precipitated iron catalysts led to a decrease in the attrition resistance of the catalysts prepared. Catalysts that had the aluminium added during the precipitation step exhibited the lowest attrition resistance. This decrease is ascribed to the formation of indentations in the particles during the spray drying step.

The synthesis behaviour of these catalysts did not show any discernable differences in terms of catalytic activity. This is ascribed to the low levels of aluminium added. The selectivity differences, increased methane and decreased ethene/ethane ratio as observed, can be explained by an increased hydrogenation functionality of the catalyst prepared with the aluminium added during the precipitation step.

The onset of reduction of the catalyst prepared with the aluminium added during the precipitation step has been found to be earlier, as indicated by the TPR results. This is also ascribed to an increase in the hydrogenation functionality of the catalyst.

# 6 REFERENCES:

Adesina, A.A.
Hydrocarbon synthesis via Fischer-Tropsch reaction: travails and triumphs
*Applied Catalysis A: General* **138** (1996), 345

Anderson, R.B.
"Catalysts for the Fischer-Tropsch Synthesis",
Van Nostrand Reinhold, New York (1956)

Austin, L.G.
A treatment of impact breakage of particles
*Powder Technology* **126** (2002), 85

British Materials Handling Board
Series on Bulk Materials Handling
Vol 5: Particle Attrition, State of the Art Review
Trans. Tech. Publications, Germany (1987), ISBN 0-87849-076-0

Bukur, D.B., Mukesh, D., Patel, S.A.
Promoter effects on precipitated iron catalysts for Fischer-Tropsch synthesis
*Industrial Engineering Chemistry Research* **29** (1990a), 194

Bukur, D.B., Lang, X., Mukesh, D., Zimmerman, W.H., Rosynek, M.P., Li, C.
Binder/support effects on the activity and selectivity of iron catalysts in the Fischer-Tropsch synthesis
*Industrial Engineering Chemistry Research* **29** (1990b), 1588

Bukur, D.B., Nowicki, L., Manne, R.K., Lang, X.
Activation studies with a precipitated iron catalyst for Fischer-Tropsch synthesis. 2: Reaction studies"
*Journal of Catalysis* **155** (1995), 366

Denny, P.J., Whan, D.A.
The Heterogeneously Catalysed Hydrogenation of Carbon Monoxide
In "Catalysis" (C Kemball, D.A. Dowden, Eds)
The Chemical Society, Volume 2, p 46. The Burlington House, (1978) London W1V 0BN: ISBN 0-85186-5445

Dictor, R.A., Bell, A.T.
Fischer-Tropsch synthesis over reduced and unreduced iron oxide catalysts
*Journal of Catalysis* **97** (1986), 121

Dlamini, H., Motjope, T., Joorst, G., ter Stege, G., Mdleleni, M.
Changes in physio-chemical properties of iron based Fischer-Tropsch catalyst induced by $SiO_2$ addition
*Catalysis Letters* **78** (2002), 201

Donnelly, T.J., Satterfield, C.N.
Product distributions of the Fischer-Tropsch synthesis on precipitated iron catalysts
*Applied Catalysis* **52** (1989), 93

Dry, M.E., Oosthuizen, G.J.
The correlation between catalyst surface basicity and hydrocarbon selectivity in the Fischer-Tropsch synthesis
*Journal of Catalysis* **11** (1968), 18

Dry, M., Shingles, T., vH.Botha, C.S.
Factors influencing the formation of carbon on iron Fischer-Tropsch catalysts. 1: The influence of promoters
*Journal of Catalysis* **17** (1970), 341

Dry, M.E.
The Fischer-Tropsch Synthesis
In "Catalysis-Science and Technology" (J.R. Anderson, M. Boudart, Eds.), Vol.1, Springer-Verlag, New York, 1981

Dry, M.E.
Catalytic aspects of industrial Fischer-Tropsch synthesis
*Journal of Molecular Catalysis* **17** (1982), 133

Dry, M.E.
Practical and theoretical aspects of the catalytic Fischer-Tropsch process
*Applied Catalysis A, General* **138** (1996), 319

Dry, M.E.
The Fischer-Tropsch process: 1950-2000
*Catalysis Today* **71** (2002), 227

Dwyer, D.J., Hardenbergh, J.H.
The catalytic reduction of carbon monoxide over iron surfaces: a surface science investigation
*Journal of Catalysis* **87** (1984), 66

Egiebor, N.O., Cooper, W.C.
Fischer-Tropsch synthesis on a precipitated iron catalyst: influence of silica support on product selectivities
*Canadian Journal of Chemical Engineering* **63** (1985), 81

Fischer, F., Tropsch, H.
Die Erdölsynthese bei gewönlichem Druck aus den Vergasungsprodukten der Kohlen
*Brenstoff-Chemie* **7** (1926), 97

Friedel, R.A., Anderson, R.B.
Composition of synthetic liquid fuels. 1. Product distribution and analysis of $C_5$-$C_8$ paraffin isomers from cobalt catalyst"
*Journal of the American Chemical Society* **72** (1950), 1212-1215

Geus, J.W.
Preparation and Properties of Iron Oxide and Metallic Iron Catalysts
*Applied Catalysis* **25** (1986), 313

Henrici-Olivé, G., Olivé, S.
The Fischer-Tropsch Synthesis: Molecular Weight Distribution of Primary Products and Reaction Mechanism
*Angewandte Chemie International Edition* **15** (1976), 136

Hess, W., Schönert, K.
Brittle-Plastic Transition in Small Particles
Proc. Powtech Conf. Particle Technology, Birmingham, 1981, EFCE Event no. 241, D2/I/1-D2/I/9.

Huang, C.S., Xu, L., Davis, B.H.
Fischer-Tropsch synthesis: impact of pretreatment of ultrafine iron oxide upon catalyst structure and selectivity
*Fuel Science & Technology International* **11** (1993), 639

Iglesia, E., Reyes, S.C., Madon, R.J.
Transport enhanced alpha olefin readsorption pathways in Ru-catalysed hydrocarbon synthesis
*Journal of Catalysis* **129** (1991), 238

Jothimurugesan, K., Goodwin, J.G. Jr., Gangwal, K.S., Spivey, J.J.
Development of Iron Fischer-Tropsch Catalysts for Slurry Bubble Column Reactors
*Catalysis Today* **58** (2000), 335

Jung, H., Thomson, W.J.
Dynamic X-Ray Diffraction Study of an Unreduced Iron Oxide Catalyst in Fischer-Tropsch Synthesis
*Journal of Catalysis* **139** (1993), 375

Kalakkad, D.S., Shroff, M.D., Kohler, S., Jackson N.B., Datye, A.K.
Attrition of Precipitated Iron Fischer-Tropsch Catalyst
*Applied Catalysis A: General* **133** (1995), 335

Kochloefl, K.;
Steam Reforming
In "Handbook of Heterogeneous Catalysis" (E. Ertl, H. Knözinger, J. Weitkamp, Eds.), Volume 4., p 1819 , Wiley VCH (1997), ISBN 3-527-29212-8

Kock, A.J.H.M.
The Characterisation of Iron Catalysts – Carbon Deposition, Reduction and Literature Survey
PhD thesis University of Utrecht, Printed by Wibro Helmond (1985)

Kock, A.J., Fortuin, H.M, Geus, J.W.
The Reduction Behaviour of Supported Iron Catalysts in Hydrogen or Carbon Monoxide Atmospheres
*Journal of Catalysis* **96** (1985), 261

Madon, R.J., Taylor, W.F.
Fischer-Tropsch Synthesis on a Precipitated Iron Catalyst
*Journal of Catalysis* **69** (1981), 32

Madon, R.J., Reyes, S.C., Iglesia, E.
Primary and secondary reaction pathways in ruthenium-catalysed hydrocarbon synthesis
*Journal of Physical Chemistry* **95** (1991), 7795

Masters, K.
"Spray Drying Handbook" 5th edition, Longman Scientific Technical, ISBN 0-582-06266-7

Mullin, J.W.
Precipitation
in "Ullmann's Encyclopaedia of Industrial Chemistry" (Elvers, B. Ravenscroft, M. Rounsaville, J.F. Schulz, G., Eds.), Vol. B2, p. , 3-35, VCH Publishers (1988), ISBN 3-527-20132-7

Motjope, T.R., Dlamini, H.T., Hearne, G.R., Coville, N.J.
Application of In-situ Mössbauer Spectroscopy to Investigate the Effect of Precipitating Agents on Precipitated Iron Fischer-Tropsch Catalyst
*Catalysis Today* **71** (2002), 335

Pham, H.N., Reardon, J., Datye, A.K.
Measuring the strength of slurry phase heterogeneous catalysts
*Powder Technology* **103** (1999), 95

Pham, H.N., Viergutz, A., Gormley, R.J., Datye, A.K.
Improving the Attrition Resistance of Slurry Phase Heterogeneous Catalysts
*Powder Technology* **110** (2000 a), 196

Pham, H.N., Datye, A.K.
The Synthesis of Attrition Resistant Slurry Phase Iron Fischer –Tropsch Catalysts
*Catalysis Today* **58** (2000 b), 233

Rao, V.U.S., Stiegel, G.J., Cincuegrane, G.J., Srivastava, R.D.
Iron-based catalysts for slurry-phase Fischer-Tropsch processes: Technology Review
*Fuel Processing Technology* **30** (1992), 83

Reppenhagen, J., Werther, J.
Catalyst attrition in cyclones
*Powder Technology* **113** (2000), 55

Röper, M.
Fischer-Tropsch synthesis
in “Catalysis in $C_1$ Chemistry” (W. Keim, Ed.), pp. 41, D. Reidel, Dordrecht, The Netherlands (1983)

Rostrup-Nielsen, J.R.
Syngas in Perspective
*Catalysis Today* **71** (2000), 243

Satterfield, C.N., Huff Jr.,G.A.
Usefulness of a slurry-type Fischer-Tropsch reactor for processing synthesis gas of low hydrogen-carbon monoxide ratios
*Canadian Journal of Chemical Engineering* **60** (1982), 159

Schlögl, R.
Bulk Catalysts and Supports
In ”Handbook of Heterogeneous Catalysis” (E. Ertl, H. Knözinger, J. Weitkamp, Eds.), Volume 1, p 54, Wiley VCH (1997), ISBN 3-527-2922-8

Pichler, H., Schulz, H., Pichler, H.
Neuere Erkenttnisse auf dem Gebiet der Synthese von Kohlenwasserstoffen aus CO und $H_2$
*Chemie-Ingenieur Technik* **42** (1970), 1162

Schulz, H.
Polymethylen aus Synthesegas
in “Chemierohstoffe aus Kohle” (J. Falbe, Ed.), pp. 335-355, Georg Thieme Verlag, Stuttgart (1977)

Schulz, H., van Steen, E., Clayes, M.
Olefin formation, hydrogenation and isomerization in the kinetic regime of Fischer-Tropsch synthesis
Proc. DGMK Conf. "Selective Hydrogenation and Dehydrogenation", Kassel, 1993 (M. Baerns, J. Weitkamp eds.), Tagungsbericht 9305, p. 139-146, DGMK, Hamburg (1993)

Schüth, F., Unger, K.
Precipitation and Coprecipitation
In "Handbook of Heterogeneous Catalysis" (E. Ertl, H. Knözinger, J. Weitkamp, Eds.), Volume 1, p 72, Wiley VCH (1997), ISBN 3-527-2922-8

Schulz. H., Beck, K., Erich, E.
Kinetices of Fischer-Tropsch Selectivity
*Fuel ProcessingTechnology* **18** (1988), 293

Schulz, H., Erich, E., Gorre, H., van Steen, E.
Regularities of selectivity as a key for discriminating FT-surface reactions and formation of the dynamic system
*Catalysis Letters* **7** (1990), 157

Schulz, H., Nie, Z., Claeys, M.
Initial episodes of Fischer-Tropsch Synthesis with Cobalt Catalyst.
*Studies in Surface Science and Catalysis* **119** (1998), 191

Schwertmann, U., Cornell, R.M.
"Iron Oxides in the Laboratory: Preparation and Characterization", 2nd ed. (2000) Wiley-VCH: ISBN 3-527-29669-7

Shroff, M.D., Kalakkad, D.S., Coulter, K.E., Kohler, S.D., Harrington, M.S., Jackson, N.B., Sault, A.G., Datye, A.K.
Activation of Precipitated Iron Fischer-Tropsch Synthesis Catalyst
*Journal of Catalysis* **156** (1995), 185

Steynberg, A.P., Espinoza, R.L., Jager, B., Vosloo, A.C.
High temperature Fischer-Tropsch synthesis in commercial practice
*Applied Catalysis A: General:* **186** (1999), 41

Storch, H.H., Golumbic, N., Anderson, R.B.
The Fischer-Tropsch and Related Synthesis
John Wiley, New York, 1951

Sudsakorn, K., Goodwin, J.G, Jr., Jothimurugesan, K., Adeyiga, A.A.
Preparation of Attrition-Resistant Spray-Dried Fe Fischer-Tropsch Catalyst Using Precipitated $SiO_2$
*Industrial Engineering Chemistry Research* **40** (2001), 4778

Vannice, M.A.
The Catalytic Synthesis of Hydrocarbons from $H_2$/CO Mixtures over the Group VIII metals. The Catalytic Behaviour of Silica-Supported Metals
*Journal of Catalysis* **50** (1977), 228

Werther, J., Xi, W.
Jet attrition of catalyst particle in gas fluidized beds
*Powder Technology* **76** (1993), 39

Zhao, R., Goodwin jr., J.G, Oukaci, R.
Attrition Assessment for Slurry Bubble Column Reactor Catalyst
*Applied Catalysis A: General* **189** (1999), 99

Zhao, R., Goodwin jr., J.G, Jothimurugesan, K., Gangwal, S.K., Spivey, J.J.
Spray Dried Iron Fischer-Tropsch Catalyst. 1. Effect of Structure on the Attrition Resistance of the Catalyst in the Calcined State
*Industrial Engineering Chemistry Research* **40** (2001a), 1065

Zhao, R., Goodwin jr., J.G, Jothimurugesan, K., Gangwal, S.K., Spivey, J.J.
Spray Dried Iron Fischer-Tropsch Catalyst. 2. Effect of Carburization on Catalyst Attrition Resistance
*Industrial Engineering Chemistry Research* **40** (2001b), 1320

Van der Laan, G.P.
Kinetics, Selectivity and Scale Up of the Fischer-Tropsch Synthesis
PhD thesis, University of Groningen, CIP-GEGEVENS Koninklijke Bibliotheek, Den Haag, ISBN 90 367 1011 1

Zimmerman, W.H., Bukur, D.B.
Reaction kinetics over iron catalysts used for the Fischer-Tropsch synthesis
*Canadian Journal of Chemical Engineering* **68** (1990), 292

## Acknowledgements

I wish to gratefully acknowledge the following organisations and individuals:

1 Prof E van Steen for his support, patience and inspiration during the compilation of this thesis.

2 The management of Sasol Technology for financial and moral support.

3 F Wepener for his assistance with catalyst preparation and spray drying.

4 The SCI laboratory personnel and the Materials Characterisation group for the XRD, TPR, jet impingement and chemical analysis.

5 The PU for CHE for performing the MIP analysis.

6 Dr T Bromfield (Sasol) and Dr D de Villiers (Sasol) for their advise and proof reading of the thesis.

7 My family and parents for their support during the duration of my theoretical studies at the University of Cape Town.